arXiv:1101.2482v2 [hep-ph] 24 Feb 2011

JLAB-THY-11-8

Deeply Virtual Exclusive Processes and Generalized Parton Distributions

Charles E. Hyde[1,2], Michel Guidal[3], and Anatoly V. Radyushkin[2,4,5]

[1] Laboratoire de Physique Corpusculaire, Université Blaise Pascal, 63177 Aubière, FRANCE
[2] Department of Physics, Old Dominion University, Norfolk VA, 23529, USA
[3] Institut de Physique Nucléaire ORSAY, 91406 Orsay, France
[4] Thomas Jefferson National Accelerator Facility, Newport News, VA,23606, USA
[5] Bogoliubov Laboratory of Theoretical Physics, 141980 Dubna, Russia

Abstract.

The goal of the comprehensive program in Deeply Virtual Exclusive Scattering at Jefferson Laboratory is to create transverse spatial images of quarks and gluons as a function of their longitudinal momentum fraction in the proton, the neutron, and in nuclei. These functions are the Generalized Parton Distributions (GPDs) of the target nucleus. Cross section measurements of the Deeply Virtual Compton Scattering (DVCS) reaction $ep \to ep\gamma$ in Hall A support the QCD factorization of the scattering amplitude for $Q^2 \geq 2$ GeV^2. Quasi-free neutron-DVCS measurements on the Deuteron indicate sensitivity to the quark angular momentum sum rule. Fully exclusive H$(e, e'p\gamma)$ measurements have been made in a wide kinematic range in CLAS with polarized beam, and with both unpolarized and longitudinally polarized targets. Existing models are qualitatively consistent with the JLab data, but there is a clear need for less constrained models. Deeply virtual vector meson production is studied in CLAS. The 12 GeV upgrade will be essential for for these channels. The ρ and ω channels reactions offer the prospect of flavor sensitivity to the quark GPDs, while the ϕ-production channel is dominated by the gluon distribution.

1. Deeply Virtual Exclusive Scattering

In the past decade, Deep Exclusive Scattering (DES) has emerged as a powerful new probe of the partonic structure of the nucleon, hadrons and nuclei. These are reactions of the type:

$$\begin{aligned} e + \text{Nucleon} &\to e + \text{Nucleon} + \gamma \\ &\to e + \text{Nucleon} + \text{meson} \end{aligned} \tag{1}$$

The $eN \to eN\gamma$ reaction is the coherent sum of the Bethe-Heitler and virtual Compton amplitudes, as illustrated in Fig. 1. The electron scattering kinematics of deeply virtual processes corresponds to the Deep Inelastic Scattering (DIS), or Bjorken limit of inclusive electron scattering, with Q^2 large and W^2 above the resonance region. In addition, the forward exclusive limit is defined kinematically by $-t \lesssim \Lambda^2_{\rm QCD} \lesssim 1$ GeV^2. Thus the deeply virtual Compton scattering (DVCS) amplitude, $\gamma^* N \to \gamma N$ is an "off-forward" generalization of the forward Compton amplitude which defines the DIS cross section via the optical theorem.

The intense interest in DVCS started after the article by Ji [1], linking DVCS to the total contribution of quarks to the proton spin. It was found [1, 2, 3, 4] that, in analogy with DIS,

in the limit of large Q^2 and small t, amplitudes of DVCS and deeply virtual meson production (DVMP) can be expressed in a power series of $1/Q^2$, with the power determined by twist (dimension minus spin) of each operator in the expansion. Detailed proofs of factorization for DVCS and DVMP were given in [5, 6, 7, 8]. This factorization is depicted in Fig. 2 for the DVCS and DVMP amplitudes. In these processes, the leading power term of the amplitude is the convolution of the perturbative kernel with a new class of non-local bi-linear twist-2 quark (or gluon) operators, called Generalized Parton Distributions (GPDs) [1, 2]. These were first described by Müller *et al.* [9]. In the case of deeply virtual meson production, the hard kernel is also convoluted with the meson Distribution Amplitude (DA).

1.1. Generalized Parton Distributions

The Generalized Parton Distributions (GPDs) parameterize Fourier transforms of nucleon matrix elements of bilinear quark (and gluon) operators separated by a light-like interval $z^2 = 0$ [9]. The kinematics are commonly defined in terms of symmetric variables (see Figs. 1 and 2) :

$$P_\mu = (p_\mu + p'_\mu)/2, \qquad \overline{q} = (q_\mu + q'_\mu)/2$$
$$\xi = \frac{-\overline{q}^2}{2\overline{q}\cdot P} \longrightarrow \frac{x_{\rm Bj}}{2 - x_{\rm Bj}} \qquad \text{as} \quad t/Q^2 \to 0. \tag{2}$$

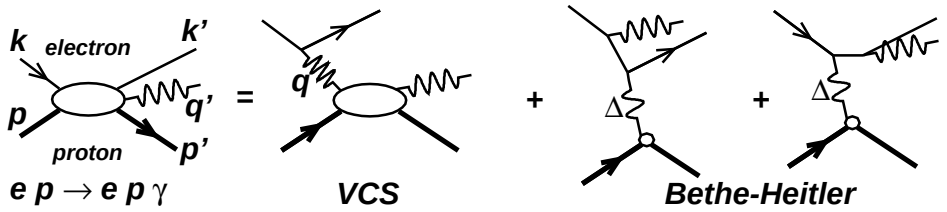

Figure 1. Lowest order QED amplitude for the $ep \to ep\gamma$ reaction. The momentum four-vectors of all external particles are labeled at left. The net four-momentum transfer to the proton is $\Delta_\mu = (q - q')_\mu = (p' - p)_\mu$. In the virtual Compton scattering (VCS) amplitude, the (spacelike) virtuality of the incident photon is $Q^2 = -q^2 = -(k - k')^2$. In the Bethe-Heitler (BH) amplitude, the virtuality of the incident photon is $-\Delta^2 = -t$. Standard (e, e') invariants are $s_e = (k + p)^2$, $x_{\rm Bj} = Q^2/(2q \cdot p)$ and $W^2 = (q + p)^2$.

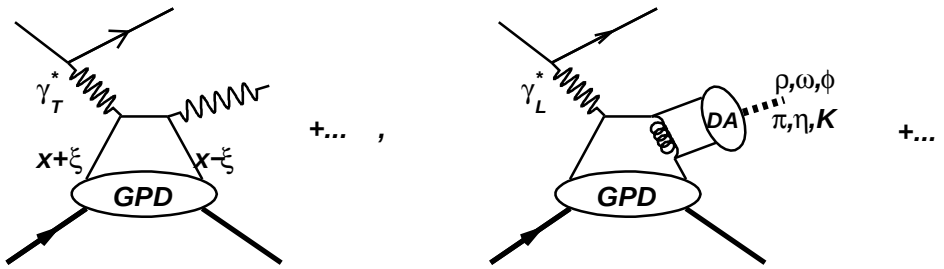

Figure 2. Factorization of the $\gamma^* p \to \gamma p$ DVCS amplitude and the $\gamma^* p \to MN$ deep virtual meson production amplitude in the Bjorken limit of large Q^2 and $-t \ll Q^2$. All permutations of the photon and gluon vertices should be included in the amplitudes. The labels on the quark lines are the light-cone momentum fractions, relative to $P^+ = (p + p')^+/2$.

The generalized Bjorken variable ξ has the same form with respect to the symmetrized variables P and $\overline{q}$ as does $x_{\rm Bj}$ with respect to the DIS variables p and q.

It is convenient to use a reference frame in which P^μ has only time- and z-components, both positive. We define light-cone vectors

$$n^\mu = [1,0,0,-1]\,/(\sqrt{2}P^+)\,, \qquad \tilde{p}^\mu = [1,0,0,1]\,P^+/(\sqrt{2}) \tag{3}$$

Then in the forward limit of either DVCS or deeply virtual production of a light meson, -2ξ is the "+" fraction of both the momentum transfer to the target and the virtual photon:

$$\Delta^+ \;\; = \Delta\cdot n \approx -2\xi P^+ \approx q\cdot n = q^+ \tag{4}$$

The quark GPDs H and E are the nucleon helicity conserving and helicity-flip matrix elements of the vector operator containing $\gamma\cdot n = \gamma^+$. Suppressing the QCD scale dependence and the Wilson-line gauge link one can write the flavor-f dependent GPDs as (see, e.g., [10]):

$$\begin{aligned}\int \frac{dz^- P^+}{2\pi} e^{ixP^+z^-}\, &\langle p',s'|\,\overline{\Psi}_f\left(-z^-/2\right)\gamma\cdot n\Psi_f\left(z^-/2\right)|p,s\rangle \\ &= \overline{U}(p',s')\left[H_f(x,\xi,t)\,\gamma\cdot n + E_f(x,\xi,t)\,\frac{i}{2M}n_\alpha\sigma^{\alpha\beta}\Delta_\beta\right]U(p,s)\;,\end{aligned} \tag{5}$$

where the $U(p,s)$ are the nucleon spinors. The factorization proofs demonstrate that the initial and final + momenta of the active parton are $(x\pm\xi)P^+$. The GPDs $\widetilde{H}$, $\widetilde{E}$ are defined similarly as the matrix elements of the axial operator containing $n\cdot\gamma\gamma_5 = \gamma^+\gamma_5$:

$$\begin{aligned}\int \frac{dz^- P^+}{2\pi} e^{ixP^+z^-}\, &\langle p',s'|\,\overline{\Psi}_f\left(-z^-\right)\gamma\cdot n\gamma_5\Psi_f\left(z^-\right)|p,s\rangle \\ &= \overline{U}(p',s')\left[\widetilde{H}_f(x,\xi,t)n\cdot\gamma\gamma_5 + \widetilde{E}_f(x,\xi,t)\frac{n\cdot\Delta}{2M}\gamma_5\right]U(p,s)\;.\end{aligned} \tag{6}$$

With the convention that positive and negative momentum fractions refer to quarks and anti-quarks, respectively, we observe the following kinematic regions of the GPDs (Fig. 2): $x>\xi>0$: the initial and final partons are quarks; $x<-\xi<0$: the initial and final partons are anti-quarks; $|x|<\xi$: a $q\overline{q}$ pair is exchanged in the t-channel. This identification is reflected in the QCD evolution equations of the GPDs. For $|x|>\xi$, the evolution of GPDs is similar to the DGLAP evolution of the forward parton distributions, whereas for $|x|<\xi$, the GPDs evolve according to the ERBL equations of a meson DA [2].

The GPDs combine the momentum fraction information of the forward parton distributions (PDFs) of DIS with the transverse spatial information of the elastic electro-weak form factors. The forward limits of the helicity conserving GPDs are

$$\left.\begin{matrix}H_f(x,0,0)\\ \widetilde{H}_f(x,0,0)\end{matrix}\right\} = \begin{cases}q_f(x)\theta(x) - \overline{q}_f(-x)\theta(-x)\\ \Delta q_f(x)\theta(x) + \Delta\overline{q}_f(-x)\theta(-x),\end{cases} \tag{7}$$

where $q_f(x)$ and $\overline{q}_f(x)$ are the flavor-f dependent quark and anti-quark momentum-fraction distributions; and $\Delta q_f(x)$ and $\Delta\overline{q}_f(x)$ are the quark and anti-quark helicity distributions. There are no specific analogous constraints on the forward limits of E and $\widetilde{E}$.

The first moments of the GPDs are equal to the corresponding elastic form factors.

$$\int dx \left\{\begin{matrix}H_f(x,\xi,t)\\ E_f(x,\xi,t)\end{matrix}\right\} = \begin{cases}F_{1,f}(-t)\\ F_{2,f}(-t)\end{cases} \tag{8}$$

where $F_{1,f}(-t)$, $F_{2,f}(-t)$ are flavor-f components of the Dirac and Pauli form factors of the proton, defined with positive arguments in the space-like regime. Similarly,

$$\int dx \left\{ \begin{array}{c} \widetilde{H}_f(x,\xi,t) \\ \widetilde{E}_f(x,\xi,t) \end{array} \right\} = \begin{cases} g_{A,f}(-t) \\ g_{P,f}(-t), \end{cases} \tag{9}$$

where $g_{A,f}$ and $g_{P,f}$ are the flavor components of the axial and pseudoscalar form factors of the proton.

The ξ-independent integrals of (8) and (9) are examples of the polynomiality condition required by Lorentz invariance. Specifically, the x^N moment of a GPD is polynomial in even powers of ξ, with maximal power $\leq (N+1)$ for H, E and maximal power $\leq N$ for $\widetilde{H}$, $\widetilde{E}$. The second moment of the GPD sum $H+E$ leads to the important angular momentum sum rule of Ji [1]:

$$\lim_{t\to 0} \int_{-1}^{1} dx\, x \left[H_f(x,\xi,t) + E_f(x,\xi,t) \right] \quad = 2J_f \,, \tag{10}$$

where $2J_f$ is the fraction of the spin of the proton carried by quarks of flavor f, including both spin and orbital angular momentum. More generally, at non-zero t, the individual second moments are form factors (i.e., Fourier transforms of spatial distributions) of the nucleon's energy-momentum tensor [1].

$$\begin{aligned} \int_0^1 dx\, x H_f(x,\xi,t) &= M_{2,f}(t) + \frac{4}{5}\xi^2 d_{1,f}(t) \\ \int_0^1 dx\, x E_f(x,\xi,t) &= [2J_f(t) - M_{2,f}(t)] - \frac{4}{5}\xi^2 d_{1,f}(t) \,. \end{aligned} \tag{11}$$

The forward limit $M_{2,f}(0)$ is the ordinary momentum sum rule

$$M_{2,f}(0) = \int_0^1 x dx \left[q_f(x) + \overline{q}_f(x) \right] \,. \tag{12}$$

The term $d_{1,f}(t)$ is Fourier conjugate to the spatial distribution of the time-averaged shear stress on quarks in the nucleon [11, 12].

The GPDs themselves, and not just the moments, provide unique spatial information about partons in the hadronic target. The parton impact parameter $\mathbf{b}$ is Fourier conjugate to $\Delta_\perp$. The Fourier transform of $H_f(x,0,\Delta^2)$ determines a positive-definite probability distribution of quarks of flavor f as a function of longitudinal momentum fraction x and spatial coordinate $\mathbf{b}$ in the transverse plane [13, 14]. As a consequence, the Dirac form factors $F_1^{p,n}$ are the 2D Fourier transforms of the charge densities of the proton and neutron in impact parameter space. A recent analysis reveals the presence of a negative charge density at the heart of the neutron[15]. In the context of the Double Distribution models of the GPDs (see section 1.3), this can be understood by the excess of down quarks over up quarks in the neutron at large x. Similarly to H, the combination of H_f and E_f at $\xi = 0$ determines the spatial density of quarks in a transversely polarized proton [16]. These distributions strongly break azimuthal symmetry about the longitudinal axis. In particular, the centroid of the up and down distributions are displaced in opposite directions, as required by the fact that the Lorentz boost of a magnetic dipole produces an electric dipole field. For $\xi \neq 0$, the Fourier transform of the GPDs determines overlap matrix elements for partons of initial and final impact parameter $\mathbf{b}/(1\pm\xi)$ with respect to the center-of-momentum of the initial and final proton [17]. In the particular $x = \xi$ case, the

variable $\mathbf{r}$, Fourier conjugate to $\Delta_\perp$, is the transverse separation of the active parton from the center-of-momentum of the spectator partons [18].

The experimental program to establish the domain of factorization in DES and to extract GPDs promises new insight into the quark-gluon structure of hadrons. The GPDs offer for the first time a probe of the rich correlations between spatial and momentum degrees of freedom of quarks and gluons in hadronic systems.

1.2. Scattering Amplitude and Observables

The $ep \to ep\gamma$ cross section has the form (Fig. 1)

$$\frac{d^5\sigma}{dQ^2 dx_{\rm Bj} d\phi_e d\Delta^2 d\phi_{\gamma\gamma}} = \frac{\alpha^3_{QED}}{4(2\pi)^2}\frac{x_{\rm Bj}y^2}{Q^4}\frac{1}{\sqrt{1+\epsilon^2_{DVCS}}}\left[|\mathcal{T}_{\rm BH}|^2 + \mathcal{I} + |\mathcal{T}_{\rm VCS}|^2\right] , \tag{13}$$

where $\epsilon^2_{DVCS} = 4x^2_{\rm Bj}M^2/Q^2$ and $\mathcal{I}$ is the BH·VCS interference term. The pure Bethe-Heitler term $|\mathcal{T}_{\rm BH}|^2$ is exactly calculable in terms of the nucleon form factors [19, 20, 21]. The full VCS amplitude is expressed as

$$\mathcal{T}_{\rm VCS}(e^\pm) = \overline{u}(k',\lambda)\gamma_\mu u(k,\lambda)\frac{(\pm e)}{q^2}H^{\mu\nu}\epsilon^\dagger_\nu \, . \tag{14}$$

The general VCS hadronic tensor H has 12 independent terms. In the leading order twist-2 approximation, H reduces to just four terms [1]

$$\begin{aligned} H^{\mu\nu}_{\rm LO,twist\,2} = \; & \tfrac{1}{2}\left(-g^{\mu\nu}\right)_\perp \overline{U}(p')\left[(n\cdot\gamma)\mathcal{H}(\xi,t) + \tfrac{i}{2M}n_\kappa\sigma^{\kappa\lambda}\Delta_\lambda\mathcal{E}(\xi,t)\right]U(p) \\ & - \left(\epsilon^{\mu\nu}\right)_\perp \overline{U}(p')\left[(n\cdot\gamma\gamma_5)\widetilde{\mathcal{H}}(\xi,t) + (\gamma_5 n\cdot\Delta)\widetilde{\mathcal{E}}(\xi,t)\right]U(p) \, , \end{aligned} \tag{15}$$

where the transverse tensors are defined as

$$\left(-g^{\mu\nu}\right)_\perp = -g^{\mu\nu} + n^\mu\tilde{p}^\nu + \tilde{p}^\mu n^\nu \, , \qquad \left(\epsilon^{\mu\nu}\right)_\perp = \epsilon^{\mu\nu\alpha\beta}n_\alpha\tilde{p}_\beta \, . \tag{16}$$

The Compton form factors (CFF) $\mathcal{H}\ldots$ in (15) are defined by the integration over the quark loop in Fig. 2:

$$\begin{aligned} \left[\mathcal{H},\mathcal{E}\right](\xi,t) &= \int_{-1}^{+1} dx \left[\frac{1}{x-\xi+i\epsilon} + \frac{1}{x+\xi-i\epsilon}\right]\left[H,E\right](x,\xi,t) \, , \\ \left[\widetilde{\mathcal{H}},\widetilde{\mathcal{E}}\right](\xi,t) &= \int_{-1}^{+1} dx \left[\frac{1}{x-\xi+i\epsilon} - \frac{1}{x+\xi-i\epsilon}\right]\left[\widetilde{H},\widetilde{E}\right](x,\xi,t) \, . \end{aligned} \tag{17}$$

Thus the imaginary parts of the CFFs are proportional to the GPDs at the point $x = \pm\xi$. Complete expressions for the VCS hadronic tensor to twist 3 accuracy are given in *e.g.*[21, 12].

The importance of the azimuthal distributions of the DVCS and interference terms, both for testing factorization and extracting constraints on the GPDs was first pointed out by Diehl *et al.*[22]. The azimuthal distribution of the DVCS and interference terms has the general form [20]

$$|\mathcal{T}_{\rm DVCS}|^2 = \frac{e^6(s_e-M^2)^2}{x^2_{\rm Bj}Q^6}\left\{\sum_{n=0}^{2} c_n^{\rm DVCS}\cos(n\phi_{\gamma\gamma}) + \sum_{n=1}^{2} s_n^{\rm DVCS}\sin(n\phi_{\gamma\gamma})\right\} \, , \tag{18}$$

$$\mathcal{I}(e^\pm) = \frac{\pm e^6 x^2_{\rm Bj}(s_e-M^2)^3}{\Delta^2 Q^2 (k-q')^2(k'+q')^2}\left\{\sum_{n=0}^{3} c_n^{\mathcal{I}}\cos(n\phi_{\gamma\gamma}) + \sum_{n=1}^{3} s_n^{\mathcal{I}}\sin(n\phi_{\gamma\gamma})\right\} \, . \tag{19}$$

The azimuthal angle $\phi_{\gamma\gamma}$ of the hadronic $\mathbf{q}' \otimes \mathbf{p}'$ plane relative to the electron scattering plane is defined such that $\sin(\phi_{\gamma\gamma}) > 0$ when $(\mathbf{k} \wedge \mathbf{k}') \cdot \mathbf{q}' > 0$ and $\phi_{\gamma\gamma} = 0$ when the final photon is on the beam side of $\mathbf{q}$.

The leading order twist-2 DVCS amplitude couples only to transverse photons. Consequently, there is a specific twist-hierarchy to the terms in (18,19) [20]:

(i) $c_0^{\rm DVCS}$, $c_0^{\mathcal{I}}$ are twist-2;
(ii) $(c,s)_1^{\mathcal{I}}$ are twist-2 (transverse VCS in interference with longitudinal BH amplitudes);
(iii) $(c,s)_1^{\rm DVCS}$ are twist-3 (LT electroproduction interference terms);
(iv) $(c,s)_2^{\rm DVCS}$, are bilinear combinations of ordinary twist-2 and gluon transversity terms;
(v) $(c,s)_2^{\mathcal{I}}$ are twist-3;
(vi) $(c,s)_3^{\mathcal{I}}$ are linear in the twist-2 gluon transversity terms.

For example, the $c, s_1^{\mathcal{I}}$ terms for unpolarized and longitudinally polarized targets are respectively:

$$\left.\begin{array}{c} c_{1,\rm unp}^{\mathcal{I}} \\ s_{1,\rm unp}^{\mathcal{I}} \end{array}\right\} \propto \left\{\begin{array}{c} \Re{\rm e} \\ \lambda \Im{\rm m} \end{array}\right\} \mathcal{C}_{\rm unp}^{\mathcal{I}} \ ,$$
$$\mathcal{C}_{\rm unp}^{\mathcal{I}} = \left[F_1 \mathcal{H} + \xi G_M \widetilde{\mathcal{H}} + \tau_C F_2 \mathcal{E}\right] \ , \tag{20}$$
$$\left.\begin{array}{c} c_{1,\rm LP}^{\mathcal{I}} \\ s_{1,\rm LP}^{\mathcal{I}} \end{array}\right\} \propto \Lambda \left\{\begin{array}{c} \lambda \Re{\rm e} \\ \Im{\rm m} \end{array}\right\} \mathcal{C}_{\rm LP}^{\mathcal{I}} \ ,$$
$$C_{\rm LP}^{\mathcal{I}} = \left[\xi G_M \left(\mathcal{H} + \frac{x_{\rm Bj}}{2}\mathcal{E}\right) + F_1 \widetilde{\mathcal{H}} - \xi \left(\frac{x_{\rm Bj}}{2} F_1 + \tau_C F_2\right) \widetilde{\mathcal{E}}\right] , \tag{21}$$

where Λ is the target polarization and $\tau_C = -\Delta^2/(4M^2)$ [20]. The EM form factors F_1, F_2, G_M are evaluated at $-t$ and the Compton form factors $\mathcal{H}$, $\mathcal{E}\ldots$ are evaluated at (ξ, t). In particular, we expect that on the proton the $F_1\mathcal{H}$ and $F_1\widetilde{\mathcal{H}}$ terms will dominate the unpolarized and longitudinal target polarization observables of (20) and (21), respectively. On the other hand, on the neutron both F_1 and $g_1(x) = \widetilde{H}(x,0,0)$ are small. We anticipate a greater sensitivity to E from the interference term on an unpolarized neutron and to the combination of $\mathcal{H}$ and $\widetilde{\mathcal{E}}$ on a longitudinally polarized neutron. Transverse target observables depend on different combinations of CFFs [20]. Dynamic and kinematic twist-3 terms in the scattering amplitude cause kinematically suppressed twist-3 terms to mix into the "twist-2" observables listed above [23, 24]. In addition, any "twist-2" observable will naturally contain contributions of all higher even-twist in a power series in $1/Q^2$. The precise twist content of DES observables must be determined via a Q^2-dependent analysis at fixed (ξ, t). A complete analysis must also include the logarithmic Q^2-dependence from QCD evolution.

1.3. Models

Several models of the GPDs exist. To varying degrees, they incorporate the theoretical and empirical constraints on the GPDs. In the valence region, the most widely used models are based on the Double Distribution (DD) ansatz proposed by Radyushkin [25]. Detailed versions of this model are presented by Vanderhaeghen, Guichon, Guidal (VGG) [26] and Goeke, Polyakov, Vanderhaeghen [21]. The Double Distributions re-parameterize the (x, ξ) dependence of the GPDs in terms of the momentum fractions β and α, of P^+ and Δ^+, respectively. Thus the initial and final parton + components of momentum are $\beta P^+ \mp (1 \pm \alpha)\Delta^+/2$. The H, E, and

$\widetilde{H}$ Double Distributions are parameterized as:

$$GPD_{f,DD}(x,\xi,t) = \int_{-1}^{+1} d\beta \int_{-1+|\beta|}^{1-|\beta|} d\alpha\, \delta(x-\beta-\alpha\xi) F_f(\beta,\alpha,t)$$
$$F_f(\beta,\alpha,0) = h(\beta,\alpha) \begin{cases} q_f(\beta); \\ \kappa_f q_f(\beta)(1-\beta)^{\eta_f}/A_f; \\ \Delta q_f(\beta); \end{cases} \tag{22}$$

for H, E, and $\widetilde{H}$, respectively. In (22) q_f and Δq_f are the ordinary and helicity-dependent parton distribution functions of flavor f and κ_f is the flavor anomalous magnetic moment of the proton. The normalization of E is such that $A_f = \int d\beta (1-\beta)^{\eta_f} q_f(\beta)$. The profile function h is commonly parameterized as

$$h(\beta,\alpha) = \frac{\Gamma(2b+2)}{2^{2b+1}\Gamma(b+1)} \frac{[(1-|\beta|)^2-\alpha^2)]^b}{(1-|\beta|)^{2b+1}} \tag{23}$$

For $b=1$, this form reduces at $\beta=0$ to an asymptotic meson DA $\Phi(\alpha) = 3(1-\alpha^2)/4$, with support $-1<\alpha<1$. This connection is suggested by the ERBL evolution equations for $|x|<\xi$. In general, the exponent b is a free parameter and for $b\to\infty$, the GPD is ξ-independent.

The DD form of (22) ensures that the polynomiality conditions are automatically satisfied. However, it was pointed out by Polyakov and Weiss that for H and E, an additional "D-term" must be included [27] to produce the highest ξ^{N+1} power for x^N moment. This term, which only has support in the ERBL region, is an iso-singlet and enters with opposite sign to H and E:

$$H_f(x,\xi,t) = H_{f,DD}(x,\xi,t) + \theta(\xi-|x|)\frac{1}{N_f} D(x/\xi,t) \ ,$$
$$E_f(x,\xi,t) = E_{f,DD}(x,\xi,t) - \theta(\xi-|x|)\frac{1}{N_f} D(x/\xi,t) \ . \tag{24}$$

In practice, the D-term has been taken as an expansion in odd Gegenbauer polynomials, with the first few terms fitted to a Chiral Soliton model calculation [28, 21]. The t dependence is introduced into the model via a Regge inspired ansatz [21]:

$$F_f(\beta,\alpha,t) \quad = h(\beta,\alpha) q_f(\beta) |\beta|^{-\alpha' t} \ . \tag{25}$$

As found in [29], the high-t form factor is dominated by the contribution in the DD at large β, for which the simple Regge forms must be modified to describe the data. A fit to all of the nucleon form factors data was obtained with the ansatz

$$F_f(\beta,\alpha,t) \quad = h(\beta,\alpha) q_f(\beta) |\beta|^{-(1-\beta)\alpha' t}. \tag{26}$$

Aside from the choice of b-parameter for each flavor and GPD, variants of the model exist with different choices of including the valence or valence plus sea contributions to E and H. The GPD $\widetilde{E}$ is generally parameterized separately, as the pion-pole in the t-channel. In this framework, $\widetilde{E}$ is directly related to the pion form factor[21, 30].

The family of models sketched above, and generically labeled "VGG" is qualitatively successful in describing the DVCS data. However, the model is highly constrained and does not have the full degrees of freedom of the GPDs. More general parameterizations will be needed as the data improves in precision and covers both a broader kinematic range and a more complete set of spin and flavor observables.

Another approach [31, 32] is to construct valence generalized parton distributions as an overlap of light-cone wave functions. However, a model involving the lowest Fock state component only produces GPDs vanishing at the border points $x = \pm\xi$ and in the whole central region $-\xi < x < \xi$ [31, 33]. It was shown [34] that inclusion of the higher Fock state components gives GPDs that are nonzero in the central region and at the border points. In particular, one may assume that overlap of the lowest Fock state components gives model GPDs at a low normalization point $Q_0 \sim 300\,\mathrm{MeV}$, and then evolve them to hard scales $Q \gtrsim 1\,\mathrm{GeV}$: the evolution will induce nonzero values for GPDs in the central region. Originally [35], the evolution approach was used to build a model for the gluon GPD, assuming that for a low normalization point Q_0 it coincides with the usual ("forward") gluon density, $H^g(x,\xi;Q_0) = xG(x,Q_0)$. In Ref. [36] this ansatz was also applied for quark distributions in an attempt to describe HERA DVCS data at low x_{Bj}, for which predictions based on the double distribution ansatz are too large in magnitude. More recently, the "Dual Parameterization" (DP) framework developed by Polyakov and collaborators [37, 38] was used to address this issue. In this approach, GPDs are expanded in terms of the partial waves exchanged in the t-channel. It was expected that for low x_{Bj} of the HERA DVCS data, the expansion may be truncated to the first "forward-like" functions [38]. However, a detailed analysis [39] demonstrated that the minimal model of the dual parameterization significantly (by a factor of 4) overestimates the HERA data. The relation between the dual parameterization approach and the double distribution ansatz was investigated in Ref. [40], where it was shown that GPDs built from DD-based models with $b = 1$ in Eq. (23) and small ξ may be reproduced just by the first term of the dual parameterization expansion, i.e., the minimal DP- and DD-based models give similar results for DVCS at small x_{Bj}, and both give a rather large value ~ 1.8 for the ratio $R^{\Sigma}(\xi) \equiv H^{\Sigma}(\xi,\xi)/\Sigma(\xi)$ of singlet quark distributions for small ξ, while experimental data favor the value close to 1. In a model developed by D. Mueller and collaborators [41] it is possible to keep the value of $R^{\Sigma}(\xi)$ "flexible", i.e. to adjust it to describe the data. The "flexibility" may be achieved also in the dual parametrization approach, if one adds the second "forward-like" function.

2. Initial DVCS Experiments

The richness of physical information in the GPDs has sparked an intense experimental effort. The H1, HERMES, and CLAS collaborations published the first evidence for the DVCS reaction in 2001.

2.1. DVCS at HERA

The H1 [42, 43, 44] and ZEUS [45, 46] collaborations measured the $p(e,e'\gamma)X$ cross section, integrated over $\phi_{\gamma\gamma}$. The exclusive $p(e,e'\gamma)p$ channel is enhanced over $p(e,e'\gamma)N^*$ channels by vetoing on forward detectors [44, 46]. In ZEUS, a subset of $p(e,e'\gamma p)$ events were tagged in a forward tracker [46]. The HERA data cover a wide kinematic range at low x_{Bj}, with central values of Q^2 and W from 8 to 85 GeV^2 and 45 to 130 GeV, respectively.

The HERMES collaboration measured the $\phi_{\gamma\gamma}$-distribution of the relative beam-helicity asymmetry in the $\mathrm{H}(\vec{e},e'\gamma)X$ reaction at average kinematics $\langle Q^2, x_{\mathrm{Bj}}, t\rangle = (2.6\,\mathrm{GeV}^2,\ 0.11,\ -0.27\,\mathrm{GeV}^2)$ [47]. The FWHM of the M_X^2 distribution was $\approx 1\,\mathrm{GeV}^2$, therefore covering the majority of the resonance region. However, at low x_{Bj} and $-t$, model estimates indicate that the exclusive $\mathrm{H}(\vec{e},e'\gamma)p$ channel is dominant[47]. The HERMES collaboration has recently measured the beam-charge asymmetry [48], transversely polarized target asymmetries [49], longitudinally polarized target asymmetries [50], and a more extensive set of beam spin asymmetries [51]. The final 2006-2007 HERMES run utilized a new recoil detector [52], to establish exclusivity via $\mathrm{H}(\vec{e},e'\gamma p)$ triple coincidence [53].

2.2. Initial CLAS DVCS Data

The JLab CLAS Collaboration first measured the relative beam-helicity asymmetry in the $H(\vec{e}, e'p)x$ reaction with 4.25 GeV incident electrons [54]. The exclusive photon was detected in only a fraction of the acceptance, due to the limited small angle acceptance of the standard CLAS calorimeter. The M_x^2 distribution is shown in Fig. 3 (left). The position and width of the exclusive $H(\vec{e}, e'p)\gamma$ event distribution was constrained to fit a subsample of $H(\vec{e}, e'p\gamma)$ data at small $(e'\gamma)$ opening angle, such that the events are dominated by the BH process. Similarly, exclusive π^0 event distributions were constrained to a subset of $H(\vec{e}, e'p\gamma\gamma)$ events from π^0 decay. Thus the $H(\vec{e}, e'p)x$ events in the exclusive region were fitted with two gaussians, for the $x = \gamma$ and $x = \pi^0$ channels. The widths and positions of these two gaussians are *a priori* constrained. In this way the exclusive $H(\vec{e}, e'p)\gamma$ channel was isolated. The resulting DVCS beam-helicity asymmetry is shown in Fig. 3 (right). The shaded band is a one-sigma fit of the form

$$\text{BSA} \quad = \alpha \sin(\phi_{\gamma\gamma}) + \beta \sin(2\phi_{\gamma\gamma}) \tag{27}$$

The α coefficient contains the twist-2 physics. The β coefficient contains the twist-3 physics, as well as contributions from $\cos(\phi_{\gamma\gamma})$ terms in the unpolarized cross section in the denominator of the beam spin asymmetry. The dashed and dotted curves in Fig. 3 are leading twist calculation of the VGG model, in the ξ-independent (at fixed x) and ξ-dependent versions, respectively [26]. The solid curve includes an estimate of twist-3 effects [55, 56]. The models, though constrained by fundamental principles are still very preliminary. It is remarkable that the data and models are in as good agreement as indicated by Fig. 3. Within the VGG model, the largest contribution to the beam helicity asymmetry on the proton comes from the $H(\pm\xi, \xi, t)$ GPD.

A second CLAS experiment, still with the standard CLAS configuration [57], measured the longitudinal target spin asymmetry in the $\vec{p}(e, e'p\gamma)$ reaction on a polarized NH_3 target [58]. In order to isolate the exclusive $ep \to ep\gamma$ events from the nuclear continuum, the statistics were limited to the triple coincidence $(e, e'p\gamma)$ events, with the photons detected in the standard CLAS calorimeter. The resulting exclusivity spectrum in Fig. 4 shows a 10:1 signal to background ratio. The longitudinal target spin asymmetry, averaged over the acceptance, is displayed in Fig. 5, for $\langle Q^2 \rangle = 1.82\,\text{GeV}^2$, $\langle \xi \rangle = 0.16$, and $\langle t \rangle = -0.31\,\text{GeV}^2$. The solid curve is a fit of the same form as (27). The resulting $\sin(\phi_{\gamma\gamma})$ moments are plotted in Fig. 6. The error bars in Figs. 5 and 6 are statistical, with the systematic errors displayed as a band at the bottom. The dashed and dotted curves in Figs. 5 and 6 indicate the sensitivity of the longitudinal target spin asymmetry to $\widetilde{H}$.

The initial success of the CLAS DVCS analysis, and the limited small angle acceptance of the CLAS calorimeter led to the construction of a small angle "Inner Calorimeter". The ongoing dedicated DVCS program in CLAS will be described in section 4.

3. The Hall A DVCS Program at 6 GeV

The Hall A DVCS program started with experiments E00-110[59] and E03-106[60]. These experiments measured, respectively, the cross sections of the $H(\vec{e}, e'\gamma)p$ and $D(\vec{e}, e'\gamma)pn$ reactions at $x_{\text{Bj}} = 0.36$ with an incident beam of 5.75 GeV. In both experiments the scattered electron was detected in the standard High Resolution Spectrometer (HRS) [61], and the photon was detected in a new 132 element PbF_2 calorimeter, subtending ~ 0.1 sr. PbF_2 is a pure Cerenkov medium, thereby minimizing the hadronic background and delivering the fastest timing pulses. All PbF_2 channels were readout by a custom 1 GHz digitizer[62], based on the ANTARES ARS0 chip[63]. The luminosity of 1–4 $\cdot 10^{37}$ Hz/cm^2 per nucleon was unprecedented for open detectors in a non-magnetic environment. The halo-free CW beam of CEBAF was essential to this success.

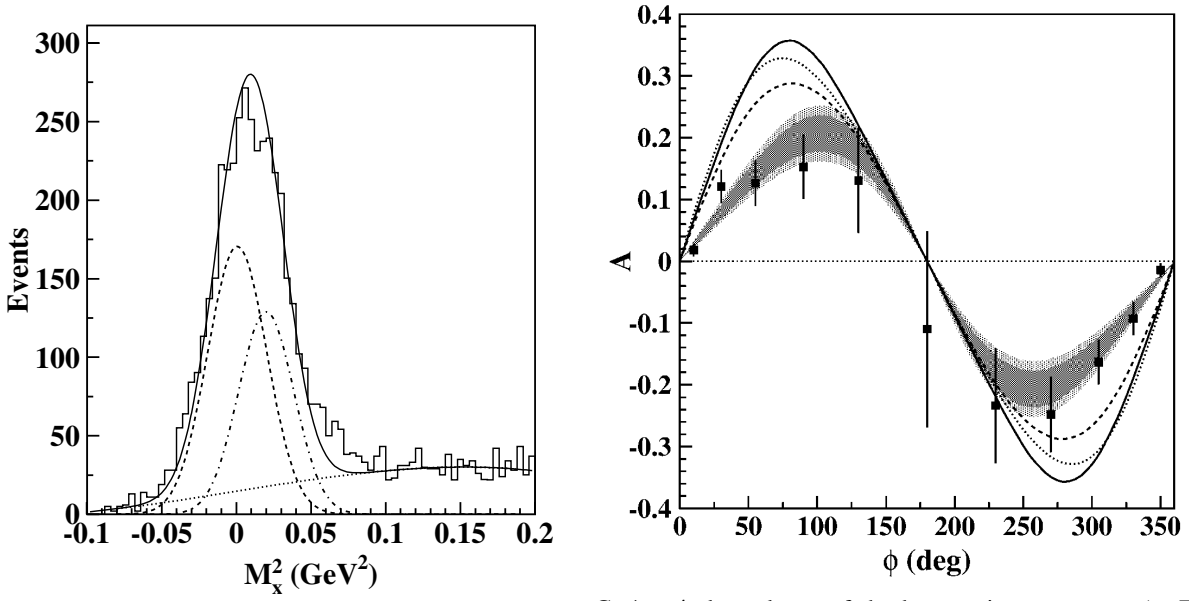

Figure 3. $H(\vec{e},e'p)x$ analysis from CLAS at 4.25 GeV incident electron energy [54]. **Left:** Missing mass squared M_x^2 distribution. The two Gaussian distributions representing the $H(\vec{e},e'p)\gamma$ and $H(\vec{e},e'p)\pi^0$ events are described in the text. The smooth polynomial background represents the contribution of processes such as $ep \to eN^*\gamma$. **Right:** DVCS Beam-helicity asymmetry. The kinematics are integrated over $Q^2 \in [1.,\, 1.75]\,\mathrm{GeV}^2$ and $-t \in [0.1,\, 0.3]\,\mathrm{GeV}^2$. The shaded region is the fit described in the text, in section 2.2. The curves, described in the text, are evaluated at the fixed values $Q^2 = 1.25\,\mathrm{GeV}^2$, $x_{\mathrm{Bj}} = 0.19$, and $t = -0.19\,\mathrm{GeV}^2$.

3.1. Proton DVCS

Hall A experiment E00-110 measured DVCS on the proton at $Q^2 = 1.5$, 1.9, and 2.3 GeV^2. The isolation of the exclusive $H(\vec{e},e'\gamma)p$ signal is illustrated in Fig. 7. The helicity dependent cross sections as a function of $\phi_{\gamma\gamma}$ in four bins in Δ^2 are displayed in Figs. 8 and 9. The latter figure also displays the helicity independent cross sections for $Q^2 = 2.3$ GeV^2. The helicity dependent cross sections demonstrate the dominance of the effective twist-2 term $s_1^{\mathcal{I}}$ of (19). The helicity independent cross sections (Fig. 9) show significant contributions from the sum of the interference and DVCS terms, in addition to the pure BH cross section. Thus the analysis of relative asymmetries of the form $\Delta\sigma/\sigma$ requires the inclusion of the full DVCS terms in both the numerator and denominator. The effective "twist-2" interference term $\Im\mathrm{m}\mathcal{C}^I$ of (20) is presented in Fig. 10. The VGG model calculation, described in section 1.3 agrees in slope with the data, but lies roughly 30% above the data. Within statistics, the results in Fig. 10 are close to Q^2-independent in all bins in Δ^2. This provides support to the conjecture that DVCS factorization results in leading twist dominance at the same scale of $Q^2 \geq 2\,\mathrm{GeV}^2$ as in DIS.

3.2. Neutron DVCS

JLab Hall A experiment E03-106 measured the helicity dependent DVCS cross section on deuterium, $D(\vec{e},e'\gamma)X$ at $Q^2 = 1.9\,\mathrm{GeV}^2$ and $x_{\mathrm{Bj}} = 0.36$. Within the impulse approximation, the cross section is described as the incoherent sum of coherent deuteron and quasi free proton and neutron channels:

$$D(\vec{e},e'\gamma) = d(\vec{e},e'\gamma)d + n(\vec{e},e'\gamma)n + p(\vec{e},e'\gamma)p + ... \tag{28}$$

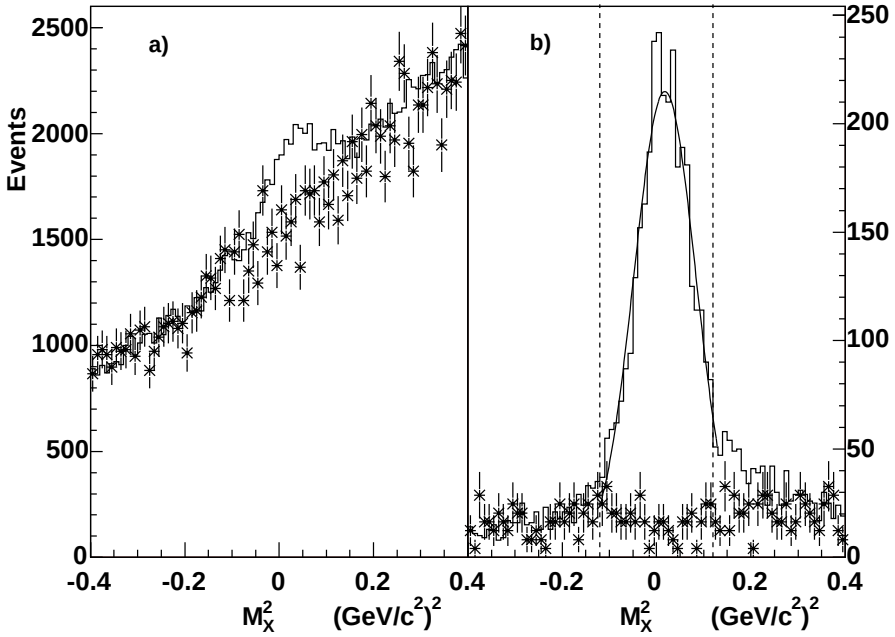

Figure 4. Missing mass squared M_x^2 distributions of the $(e, e'p)x$ reaction for $(e, e'p\gamma)$ events on a longitudinally polarized $\vec{\mathrm{NH}}_3$ target. **Left:** Raw distribution; **Right:** Distribution after requiring detected photon within 2° of the predicted direction of an exclusive photon from the $(e, e'p)\gamma$ kinematics. In both Figs. the stars are the corresponding distributions from a C target, normalized to the negative M_x^2 region.

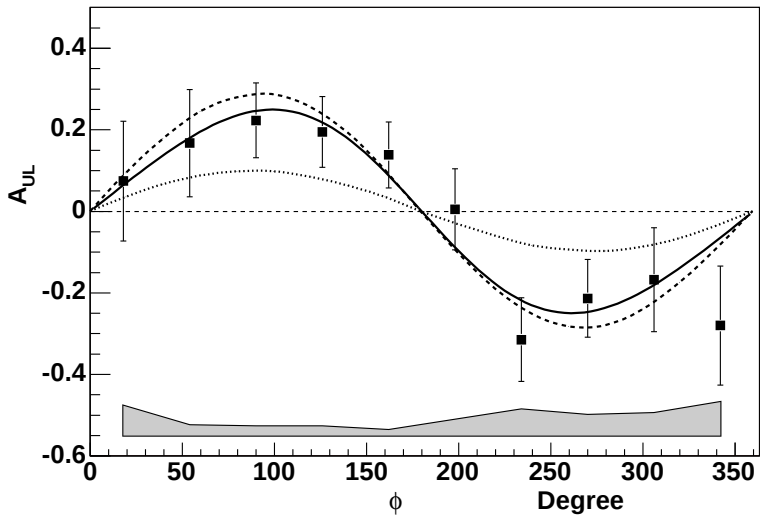

Figure 5. CLAS Longitudinal target spin asymmetry, A_{UL} [58], for $\langle Q^2 \rangle = 1.82\,\mathrm{GeV}^2$, $\langle \xi \rangle = 0.16$, and $\langle t \rangle = -0.31\,\mathrm{GeV}^2$. The solid curve is a fit of the form of (27). The dashed and dotted curves are from the ξ-dependent VGG model with $E = \widetilde{E} = 0$. The dotted curve includes only H. The dashed curve includes both H and $\widetilde{H}$.

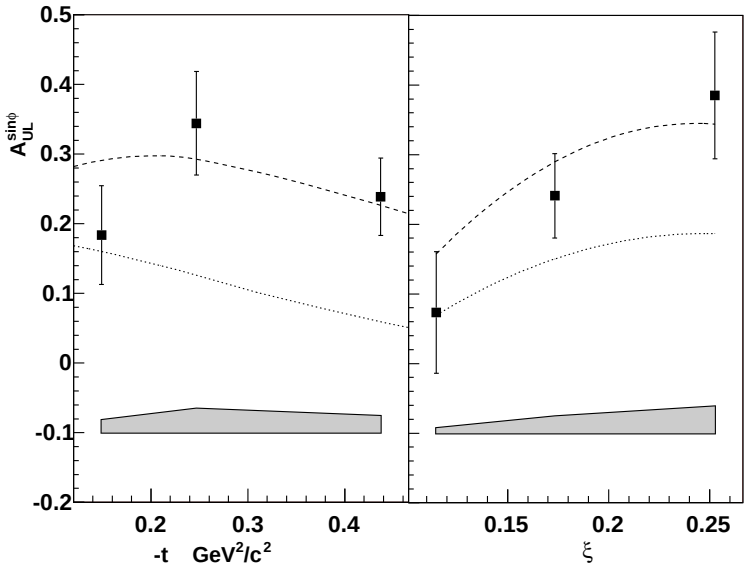

Figure 6. The $\sin(\phi_{\gamma\gamma})$ moments of A_{UL} [58]. **Left:** Three bins in $-t$, integrated over ξ; **Right:** Three bins in ξ, integrated over t. The curves are described in Fig. 5.

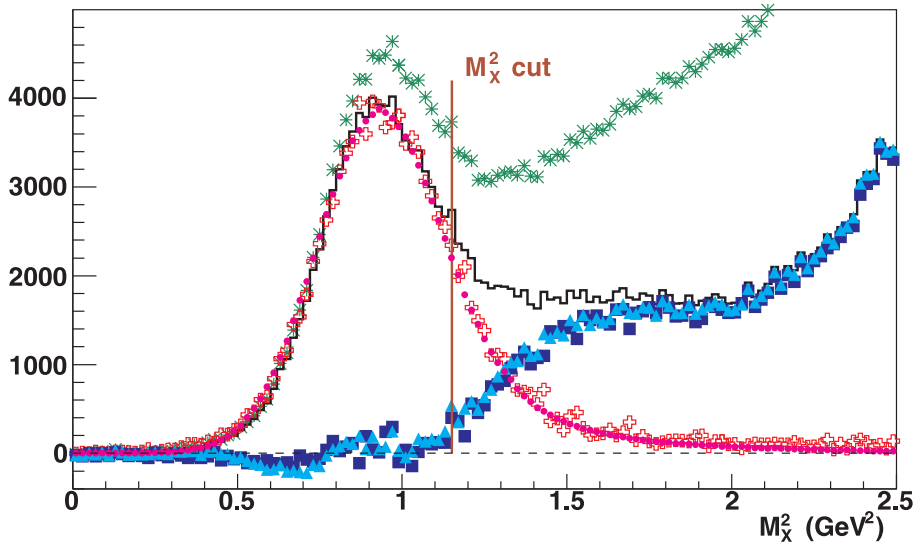

Figure 7. Missing mass squared distribution of the $\mathrm{H}(e,e'\gamma)X$ reaction in JLab Hall A experiment E00-110 [64]. The [green] stars are the raw data after accidental subtraction. The continuous [black] histogram is the data after subtracting the statistical sample of $\mathrm{H}(e;e'\gamma)\gamma X'$ events inferred from the measured $\mathrm{H}(e,e'\pi^0)X'$ sample. The open [red] cross histogram is a normalized sample of $\mathrm{H}(e,e'\gamma p)$ events. The [magenta] dots are the exclusive simulation. The [blue] triangles and squares are obtained by subtracting the last two histograms from the solid [black] histogram.

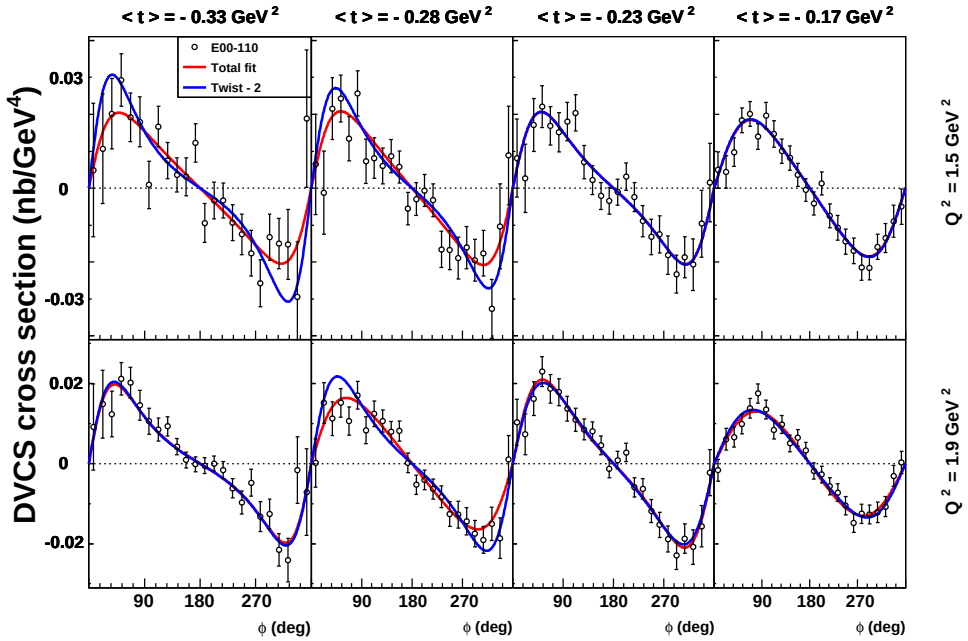

Figure 8. Helicity dependent DVCS cross sections $\Delta^4\sigma/[dQ^2 dx_{\rm Bj} d\Delta^2 d\phi_{\gamma\gamma}]$ from JLab Hall A E00-110 [64] at $Q^2 = 1.5$, and 1.9 GeV^2. The mean values of $-\Delta^2$ are, from right to left 0.17, 0.23, 0.28, and 0.33 GeV^2. Each distribution is fitted with the form of (19), with the (effective) twist-2 term in red and the complete fit in blue.

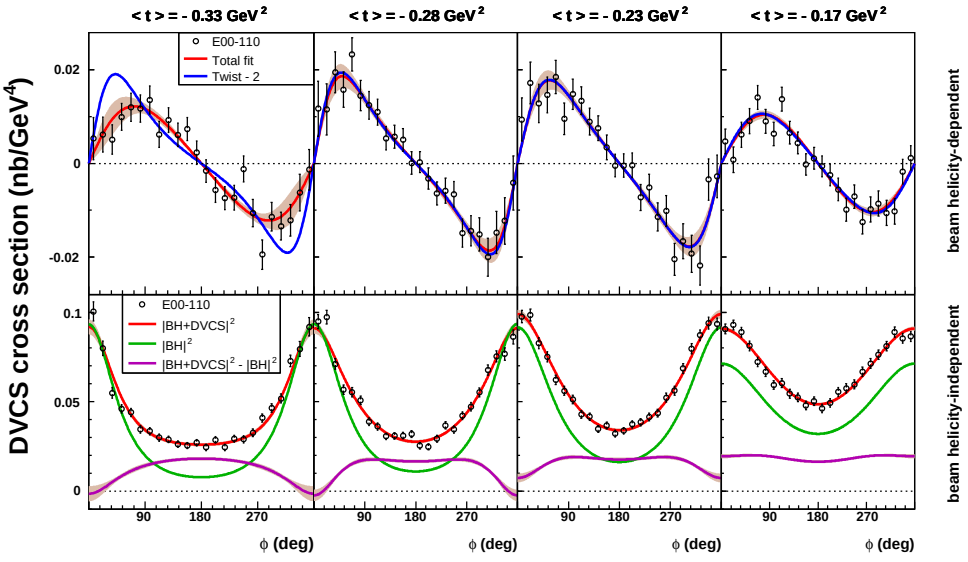

Figure 9. Helicity dependent (top) and independent (bottom) DVCS cross sections from JLab Hall A at $Q^2 = 2.3$ GeV^2 [64]. The bins are the same as Fig. 8, as are the curves in the top plot. In the bottom plot, the green curve (mostly concave up) is the pure $|{\rm BH}|^2$ cross section. The magenta curve (mostly concave down) is a fit including the twist-2 and twist-3 terms of (18, 19).

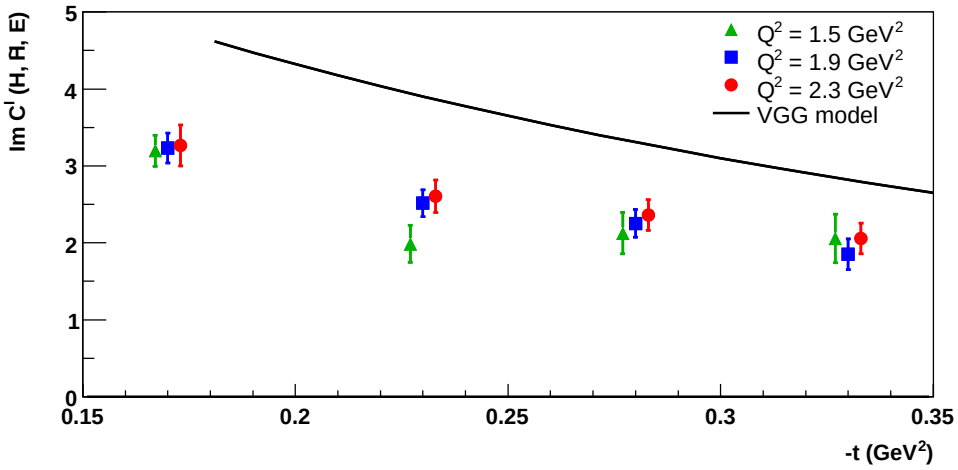

Figure 10. Imaginary part of the effective interference term $C^{\mathcal{I}}_{\rm unp}$ extracted from the helicity dependent data of Figs. 8 and 9.

Meson production channels contribute as background. The proton-DVCS contribution is calculated by smearing the H$(e,e'\gamma)X$ data by the nucleon momentum distribution in the deuteron. This statistical estimate of the proton contribution is subtracted from the data. The coherent deuteron and quasi free neutron channels were separated, within statistics, by fitting the missing mass distribution with a Monte Carlo simulation of these two channels. This separation exploits the fact that for M_X^2 calculated relative to a nucleon target, the quasi free neutron spectrum peaks at $M_X^2 \approx M^2$ whereas the coherent deuteron peak lies at $M^2+t/2$. This analysis produced constraints on the neutron and deuteron DVCS†BH interference terms $\Im{\rm m}[C^{\mathcal{I}}_{\rm unp}]$ [65]. Mazouz *et al.,* [65] fitted the neutron interference signal by varying the parameters of the E GPD within the VGG model of [21]. This results in a model dependent constraint on the Ji sum rule values of (J_d, J_u), illustrated in Fig. 11. A similar constraint obtained by the HERMES collaboration in DVCS on a transversely polarized proton target is also illustrated in the figure. Both of these experimental determinations are essentially constraints on the model at one value of $x_{\rm Bj}$, and then the model is integrated over x at fixed ξ to obtain the sum rule estimate. Measurements over a more extensive range in ξ with a more complete set of spin observables, and models with more degrees of freedom are necessary in order to more fully constrain the sum rule with realistic error bars. Lattice QCD calculations, and other phenomenological estimates are also illustrated in Fig. 11.

3.3. Future Hall A Program at 6 GeV

The unpolarized cross sections in Fig. 9 are not fully dominated by the pure BH process. The harmonic $\phi_{\gamma\gamma}$ structure of the cross section does not allow the full separation of the $\Re{\rm e}$[DVCS†BH] and $|{\rm DVCS}|^2$ contributions. These terms can be separated either by the beam charge dependence (*e.g.* [48]) or by measuring the incident energy dependence of the cross sections. At fixed Q^2, $x_{\rm Bj}$, the DVCS, Interference, and BH terms in the cross section scale roughly as $s_e^2 : s_e : 1$ (18, 19). Experiment E07-007 [71] will measure the DVCS helicity independent cross sections in the three kinematics of Figs. 8 and 9 at two separate beam energies in each kinematics. This will measure the Q^2 dependence of the separated leading twist-2 and twist-3 observables of the $\Re{\rm e}$[DVCS†BH] and $|{\rm DVCS}|^2$ terms.

Experiment E08-025 [72] will measure the DVCS cross sections on the deuteron at the same $(Q^2, x_{\rm Bj})$ value as in E03-106, but at two incident beam energies. Together with an expanded

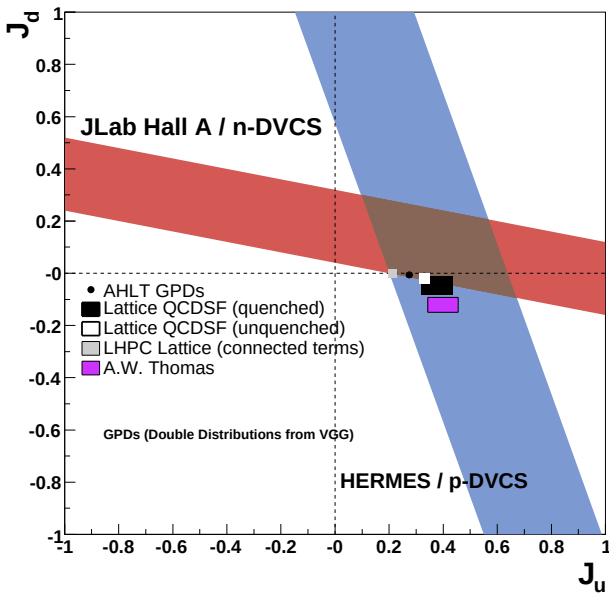

Figure 11. Experimental constraints on the total up and down quark contributions to the proton spin. JLab Hall A neutron [65] and HERMES transversely polarized proton [49]. The theory/model values are from AHLT [66], QCDSF quenched [67] and unquenched [68] LHPC [69], and Thomas [70].

calorimeter to improve the neutral pion subtraction, the two beam energies will allow a more complete separation of the DVCS^2 and real and imaginary parts of the DVCS·BH interference on a quasi-free neutron. This will be an important step towards a full flavor separation of DVCS. Both experiments E07-007 and E08-025 are running in Autumn 2010.

4. The CLAS DVCS Program at 6 GeV

4.1. Unpolarized Proton Targets

A new calorimeter of 424 tapered $PbWO_4$ crystals was constructed to provide complete 2π photon coverage for polar angles from 4.5° to 15°, relative to the beam line. A $\approx$ 5 Tesla superconducting solenoid was added at the target, to confine Moeller electrons. The new calorimeter is located 60 cm from the target where the solenoid fringe field is still a few Tesla. Therefore, the individual crystals were read-out by Avalanche Photo-Diodes. Having strongly benefited from the CERN CMS pioneering research and development effort on this recent technology, the present CLAS experiment is the first one to use such photodetectors in a physics production mode.

All particles of the $ep \to ep\gamma$ reaction final state were detected in CLAS. To ensure exclusivity, several cuts were made, a couple of them being illustrated in Fig.12. In spite of these very constraining cuts, some contamination from the $ep \to ep\pi^0$ reaction remained. Indeed, when one of the two γ's originating from the decay $\pi^0 \hookrightarrow \gamma\gamma$ escapes detection and/or has little energy (below the 150 MeV threshold of the calorimeter), an event $ep \to ep\gamma(\gamma)$ may pass all DVCS cuts and become a perfect candidate to be selected as an $ep \to ep\gamma$ event. Such "1-γ" π^0 background can be estimated from Monte-Carlo combined with the actual number of detected "2-γ" π^0's, resulting, depending on the kinematics, in contaminations ranging from 1 to 25%, being 5% in average.

The extensive CLAS dataset of DVCS beam spin asymmetries (BSA) is illustrated in Fig. 13. The blue solid curves are the result of the twist-2 handbag GPD calculation (VGG) including

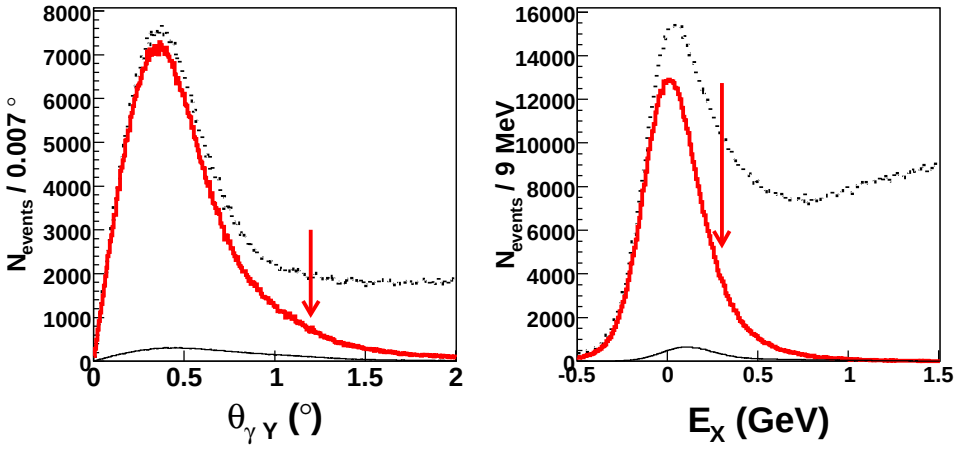

Figure 12. Example of exclusivity cuts (given by the location of the arrow) for the CLAS DVCS experiment[73]. Distribution in cone angle $\theta_{\gamma Y}$ for the $ep \to epY$ reaction (left) and in missing energy E_X for the $ep \to ep\gamma X$ reaction (right) before (black-dotted curve) and after (red solid) kinematic cuts (including others not displayed here). The thin solid black line represents the background from the $ep \to ep\pi^0$ events. These distributions are integrated over all kinematics variables.

just the H GPD [26, 29]. The blue dashed curves include the associated twist-3 calculation. Although the general trends of the data are reproduced, the model tends to overestimate the BSAs. These too large BSAs by the VGG model can come from either an overestimation of $\mathcal{H}(\xi,t)$ (the dominant factor in the numerator of the BSA) or an underestimation of the CFFs associated to the real part of the DVCS amplitude, which contribute predominantly to the denominator of the BSA [74]. The dashed black curve (third curve in some panels of Fig.13) is the result of a Regge model [75] for the DVCS process. As Q^2 increases, the Regge model drops significantly below both the data and the VGG calculations. This experiment was continued in 2008–2009, which will significantly improve the statistical precision, relative to Fig.13 [76].

4.2. Polarized Targets

In 2009, a new DVCS experiment completed data taking with the longitudinally polarized NH_3 target [77]. Relative to the previous experiment ([58] and Figs. 4–6), this new experiment will improve both the statistics and acceptance by the addition of the new electromagnetic calorimeter mentioned in the previous section. We recall that the target spin asymmetry is mostly sensitive to $\widetilde{\mathcal{H}}(\xi,t)$ and that, therefore, strong constraints on this CFF should arise from this experiment, as discussed *e.g.* in [78].

After decades of development, the HD-ice target ran successfully at the BNL-LEGS facility in 2005 and 2006. This target has now been transferred to JLab and is being prepared for a photo-production run in 2011 [79]. Initial studies of local depolarization by microwaves suggest that the spin relaxation times of this target are sufficiently long for the target to operate with electron beams in CLAS. An electron beam test is projected for the end of the 2011 photo-production run. If successful, a full suite of transverse polarization observables for the DVCS process will be feasible in CLAS in 2011. When combined with the cross section and longitudinal polarization data, along with the resulting double polarization observables, a full separation of the real and imaginary parts of all four Compton Form Factors $\mathcal{H}(\xi,t)$, $\mathcal{E}(\xi,t)$, $\widetilde{\mathcal{H}}(\xi,t)$, and $\widetilde{\mathcal{E}}(\xi,t)$ is in principle possible [20, 74].

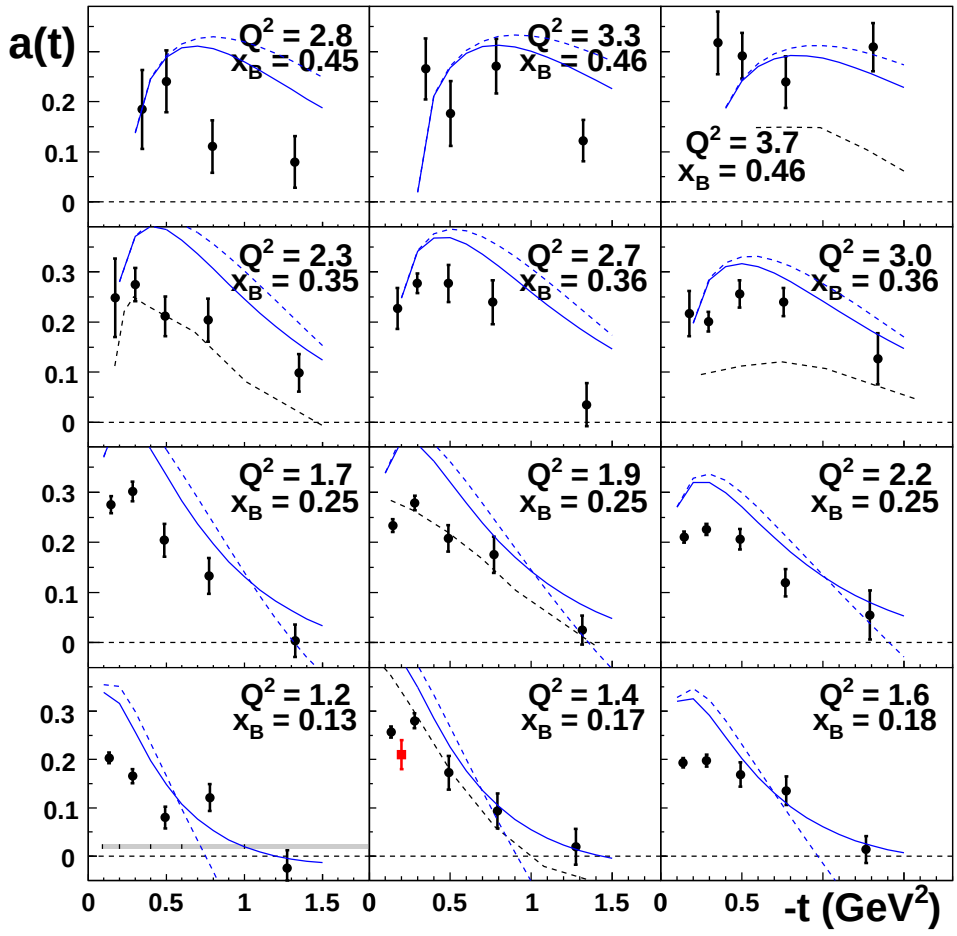

Figure 13. Beam spin asymmetry $\sin(\phi_{\gamma\gamma})$ moments from the CLAS DVCS experiment [73]. Curves are described in the text.

4.3. Nuclear Targets

GPDs are also defined for nuclei [80, 81]. One can study effects similar to the EMC effect observed for standard inclusive parton distributions functions (PDF) where the PDF of a nucleus is not simply the sum of the individual nucleon PDFs. A pioneering experiment [82, 83] of coherent DVCS on a ^{4}He target ran with the CLAS detector in 2010. ^{4}He is a very good starting case study as it is dense enough to generate nuclear medium effects, many microscopic calculations for its nuclear structure and dynamics exist and, as a global spin-0 object, at leading-twist, there is only one GPD. This ^{4}He-DVCS experiment detected the scattered electron in CLAS, the final state photon with the $PbWO_4$ and standard calorimeters mentioned in the previous sections and the recoil nucleus with a radial time-projection chamber [84]. The ϕ-distribution of the coherent DVCS BSA, up to twist-3 corrections, can yield the real and imaginary parts of the Compton Form Factor of the coherent GPD.

5. Deeply Virtual Meson Production

GPDs are in principle also accessible through exclusive meson electroproduction (see Fig. 2). With respect to the DVCS process, a few features are proper to the meson channels:

- The factorization holds only for the longitudinal part of the amplitude which implies to separate, experimentally, the transverse and longitudinal parts of the cross section. For

pseudo-scalar mesons, this can be done through a Rosenbluth separation. For vector mesons, this separation can be carried out, relying on the s-channel helicity conservation (SCHC) concept, by measuring the angular distribution of the vector meson decay products.

- In comparison to the DVCS handbag diagram, there is now a perturbative gluon exchange. This suggests that factorization will be obtained at a higher scale in exclusive meson production than in DVCS.
- Besides the GPDs, there is another non-perturbative object entering the meson handbag diagram, the meson distribution amplitude (DA). It is usually taken as the asymptotic DA but it potentially adds a further unknown in the process.
- As a positive point, the meson channels have the advantage of filtering certain GPDs: the vector meson channels are sensitive, at leading twist, only to the H and E GPDs while the pseudoscalar mesons are sensitive only to the $\tilde{H}$ and $\tilde{E}$ GPDs. Deeply virtual meson production also offers a flavor filter of the GPDs. For example, ρ^0 and ω electroproduction are sensitive to different combinations of the up- and down-quark GPDs.

Exclusive π^0 electroproduction results have been published from CLAS [85] and Hall A [86]. The Hall C results on exclusive π^+ production are discussed in the "Transition to Perturbative QCD" chapter of this volume [87]. In this section, we focus on exclusive vector meson production.

5.1. The ρ^0 channel

Deeply virtual electroproduction of the ρ^0 was studied by the CLAS collaboration at incident energies of 4.2 GeV [88] and 5.75 GeV [89]. To select the $e^-p \to e^-p\rho^0 \hookrightarrow \pi^+\pi^-$ channel, the scattered electron, the recoil proton and the π^+ were detected. A cut on the missing mass $ep \to ep\pi^+X$ was then used to identify the $e^-p \to e^-p\pi^+\pi^-$ final state. The main challenge in this analysis was to subtract under the broad ($\Gamma_{\rho^0} \approx 150$ MeV) ρ^0 peak, the non-resonant $e^-p \to e^-p\pi^+\pi^-$ (physical) background, arising for instance from processes such as $e^-p \to e^-\pi^-\Delta^{++} \hookrightarrow p\pi^+$. These "background" channels led to uncertainties of the order of 20% to 25% on the extracted cross sections.

The separation of the longitudinal and transverse parts of the cross section was carried out, as mentioned earlier, by studying the angular distribution of the decay pions in the center of mass of the $\pi^+\pi^-$ system. At the same time, by the analysis of various azimuthal angular distributions, SCHC was verified experimentally at the $\approx 20\%$ level. The longitudinal part of the $\gamma^*p \to p\rho^0$ cross section, which can in principle lend itself to a GPD interpretation, is displayed in Fig. 14 along with the world data.

The cross sections clearly exhibit two different behaviors as a function of W. At low W, the cross sections decrease as W increases ($x_{\rm Bj}$ decreases) and then begin to rise slowly for $W > 10$ GeV. These two kinematic regimes can be identified, simply speaking, with regimes of t-channel exchange of Reggeon or $q\bar{q}$ exchange in the former case and of Pomeron or 2-gluon exchange in the latter case. The results of the calculations of the JML [93] model, based on Reggeon exchange and hadronic degrees of freedom, and of the VGG [26] and GK [90, 91] models based on GPDs and on the handbag diagram of Fig. 2 are shown in Fig.14. At lower W values, where the new CLAS data lie, it is striking that both the GK and VGG models fail to reproduce the data even though they are very successful at large W, even at $Q^2 \approx 2.3\,{\rm GeV}^2$. In the high-$W$ (low $x_{\rm Bj}$) region, the gluon GPD calculations already contain large higher-twist effects in the form of intrinsic $k_\perp$ effects. The question then arises whether the higher twist effects have a different nature in the region dominated by quark GPDs (low W), or whether the double distribution based GPD models are missing an essential contribution. Ideas for such "missing" contribution in the D-term of the GPDs are speculated in [89, 92], leading to the thick solid curve in Fig. 14.

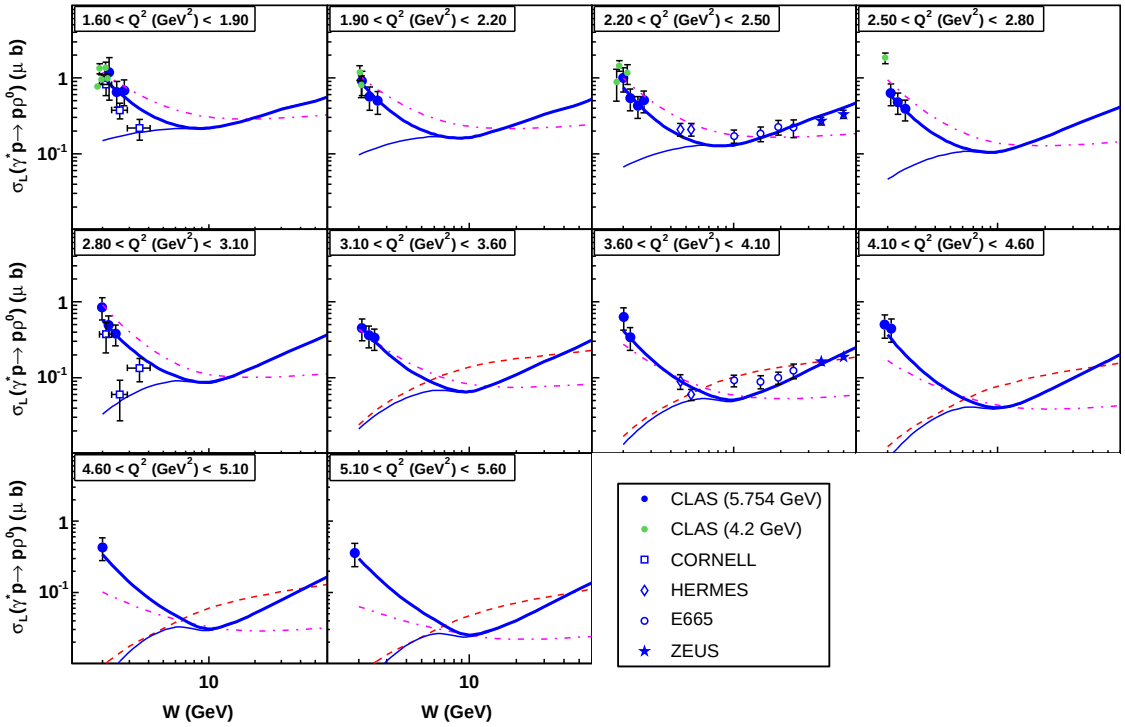

Figure 14. World data (for $W < 50$ GeV) for the reduced cross sections $\gamma_L^* p \to p\rho_L^0$ as a function of W for constant Q^2 bins (μb). The dashed curve (GK) [90, 91] and the thin solid curve (VGG) [26] are GPD calculations. The thick solid curve is the VGG calculation with the addition of the D-term inspired contribution [89, 92]. The dot-dashed curve is the Regge JML [93] calculation. The 5.75 GeV CLAS, 4.2 GeV CLAS, CORNELL, HERMES, FermiLab and ZEUS data are respectively from refs. [89], [88], [94], [95], [96], and [97].

5.2. The ω channel

The ω channel was studied in CLAS by detecting the $e^- p \to e^- p\pi^+ X$ and $e^- p \to e^- p\pi^+\pi^- X$ topologies [98]. The former is advantageous to determine total cross sections with high statistics and the latter is necessary to measure the distribution of the decay products of the ω to separate the longitudinal and transverse parts of the cross section if SCHC is verified. However, one important result of this experiment was that many SCHC-violating spin density matrix elements were measured to be significantly different from 0 in ω electroproduction. Therefore, the longitudinal and transverse parts of the cross sections were not separated. Also, the angular analysis revealed the importance of unnatural parity exchange in the t-channel, such as π^0 exchange.

In terms of quantum numbers, the π^0 exchange contribution can be identified to the $\tilde{E}$ GPD. In the framework of the JML model [104], t-channel π^0 exchange is a major contributor to the cross section. The suggested importance of π^0-exchange is in apparent contradiction with the theoretical prediction that, at sufficiently large Q^2, exclusive vector meson production should be mostly longitudinal and sensitive only to H and E. Therefore, in order to study the GPD formalism in ω production, it is essential to experimentally isolate the purely longitudinal cross section, via a Rosenbluth separation. The VGG calculation of σ_L, shown in Fig.15, lies well below the unseparated data. This suggests that a precision extraction of σ_L via a Rosenbluth separation will be a difficult experimental challenge.

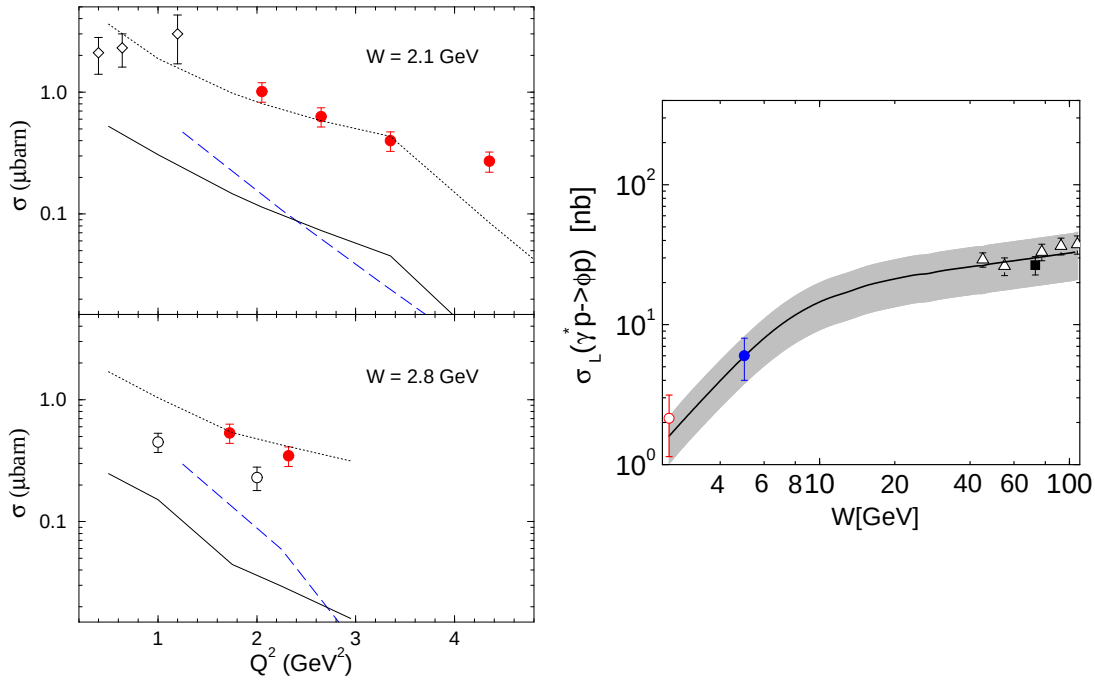

Figure 15. **Left:** Total (unseparated) cross section for the reaction $\gamma^* p \to p\omega$, for $\langle W \rangle$=2.1 GeV (top) and $\langle W \rangle$=2.8 GeV (bottom), as functions of Q^2. The dotted curve is the JML model for the total cross section $\sigma_T + \epsilon\sigma_L$ and the solid (dashed) curves shows the result of the JML (VGG) calculation for $\epsilon\sigma_L$. Data are from CLAS (full circles) [98], DESY (empty diamonds) [99] and Cornell (empty circles) [94]. **Right:** Longitudinal $\gamma^* p \to p\phi$ cross section as a function of W at Q^2=3.8 GeV^2. Data from CLAS (open circle) [100], HERMES (solid circle) [101], ZEUS (open triangles) [102] and H1 (solid square) [103]. (Courtesy of P. Kroll and S. Goloskokov).

5.3. The ϕ channel

The $e^- p \to e^- p\phi \hookrightarrow K^+K^-$ reaction was identified in CLAS by detecting the scattered electron, the recoil proton and the positive kaon and cutting around the missing mass of a kaon [100]. Relying on the SCHC concept, which was experimentally verified to hold in this channel, the longitudinal/transverse separation of the cross section was carried out. Fig 15 shows the resulting longitudinal total cross section at $Q^2 = 3.8$ GeV^2, along with higher energy HERMES and HERA data at comparable Q^2.

Exclusive ϕ electroproduction on the proton can be interpreted in terms of the handbag diagram with *gluonic* GPDs. Fig 15 shows the result of such calculation in the framework of the GK model [90, 91]. The very good agreement between this GPD calculation and the data gives confidence in the way higher twists corrections are handled, *i.e.* by taking into account the intrinsic transverse momentum dependence of the partons in the handbag calculation.

This set of three experiments delivered the largest ever dataset on vector meson production in the large Q^2 valence region. Although conclusions for the meson channels are more challenging than for DVCS, there may be the possibility to interpret the ρ^0 and ϕ channels in terms of the handbag diagram, though with large higher-twist corrections and possibly modifications of the Double-Distribution based GPD parametrisations. The higher Q^2 data from JLab at 12 GeV, as well as a global analysis including the larger DVCS dataset anticipated in the coming years should greatly clarify the role of factorization in deep virtual vector meson production.

6. Outlook

6.1. Jefferson Lab at 12 GeV

The JLab 12 GeV project offers an unprecedented frontier of intensity and precision for the study of deep exclusive scattering. The design luminosity of the upgraded CLAS12 detector is $10^{35}/\mathrm{s\,cm^2}$, with a large phase space acceptance for simultaneous detection of DVCS and deeply virtual meson production channels. At this luminosity, the Hall B dynamic nuclear polarization NH_3 target will achieve a longitudinal proton polarization of 80%. The Hall A and Hall C spectrometers will allow dedicated studies at luminosities $\geq 10^{37}/\mathrm{s\,cm^2}$ for neutral channels γ, π^0 at low t and up to $4 \cdot 10^{38}/\mathrm{s\,cm^2}$ for charged channels $\pi^{\pm}$, $K^{\pm}$. Specific 12 GeV experiments on hydrogen are approved in Hall A for DVCS (E12-06-114), in Hall B for DVCS (E12-06-119), and deep virtual π^0, η production (E12-06-108), and in Hall C for deep virtual π^+ production (E12-06-101, E12-07-105). Detailed descriptions of these experiments are available on the Hall A, B, and C web pages at `www.jlab.org`. The projected kinematic range of the DVCS programs in Hall A and B is illustrated in Fig.16. With CLAS12, additional studies are in progress for measurements of deep virtual vector meson production, neutron DVCS via $\mathrm{D}(e, e'\gamma n)p$ (LOI-09-001), coherent deuteron DVCS (PR-06-015) and DVCS on transversely polarized protons.

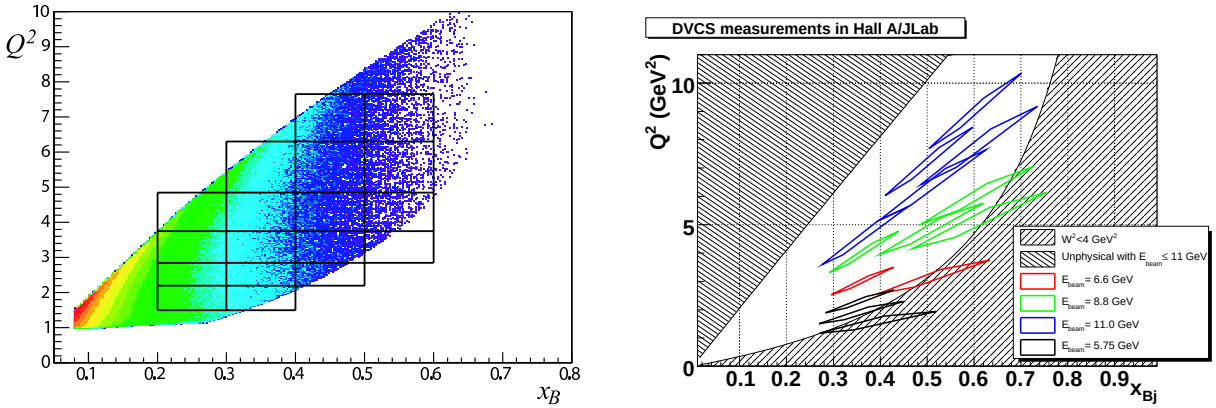

Figure 16. Projected kinematic bins at JLab 12 GeV; **Left:** CLAS12 kinematics for DVCS and DVMP on unpolarized H_2 and longitudinally polarized NH_3 targets. The colors and density are proportional to the relative count rates. **Right:** Hall A kinematics for DVCS and π^0 electroproduction. Beam time is adjusted for roughly equal counts in all bins.

6.2. Beyond 12 GeV

The COMPASS experiment at CERN proposes to measure DVCS in high energy muon scattering at low x_{Bj} via triple coincidence $\mathrm{H}(\vec{\mu}^{\pm}, \mu^{\pm}, \gamma p)$ detection [105]. The muon beams have the particularity that the muon spin and charge are correlated, enabling measurements of the DVCS†·BH interference via correlated beam charge-spin asymmetries. In addition to the COMPASS spectrometer, exclusivity will be determined by detecting the recoil protons in a scintillation array surrounding the target. The expected (correlated) range for DVCS and exclusive vector meson production is $x_{\mathrm{Bj}} \in (0.03, 0.25)$ and $Q^2 \in (1.5, 7.5)\,\mathrm{GeV}^2$. A future electron ion collider, with luminosity several orders of magnitude higher than HERA would greatly expand the reach of GPD studies. Maximizing the luminosity is essential to measure fully differential cross sections in all kinematic variables. A collider can deliver both longitudinally and transversely polarized beams without the accompanying background of unpolarized nuclei of polarized targets. A collider would also offer enhanced opportunities for spectator tagging to measure neutron GPDs, and recoil tagging for nuclear GPDs.

6.3. Conclusions

Deep virtual exclusive scattering offers the tantalizing prospect of forming spatial images of quarks and gluons in the nucleon. The GPD formalism has already given us new insight into nucleon structure, with evidence for quark angular momentum emerging from GPD models and lattice calculations, and global analysis of forward parton distributions and electromagnetic form factors. A very important study of DVCS and DES in the valence region has started with JLab at 6 GeV and will expand with the 12 GeV upgrade. Several systematic analysis demonstrate the important constraints on individual GPDs of the proton and neutron obtained from the data [41, 78, 106]. The unprecedented quality of the CEBAF continuous wave beam is essential to achieving full exclusivity at high luminosity. The revolution in polarized beams and targets over the past two decades allows us a full study of the spin degrees of freedom of DES. Over the next decade, JLab and COMPASS will obtain new precision DVCS data spanning a factor of 20 in $x_{\rm Bj}$, and at each value of $x_{\rm Bj}$, a factor of two in Q^2, with maximal Q^2 from 4 to 10 GeV^2. The present JLab data are fully differential in Q^2, $x_{\rm Bj}$ and t, allowing a systematic study of the approach to scaling in both cross section and asymmetry observables.

Acknowledgments

This work was supported by US DOE and French CNRS/IN2P3 and ANR. The authors thank our colleagues whose spirited conversations have sharpened and deepened our understanding of this subject.

This paper is authored by Jefferson Science Associates, LLC under U.S. DOE Contract No. DE-AC05-06OR23177.

References

[1] Ji X D 1997 *Phys. Rev. Lett.* **78** 610–613 (*Preprint* hep-ph/9603249)
[2] Radyushkin A V 1996 *Phys. Lett.* **B380** 417–425 (*Preprint* hep-ph/9604317)
[3] Radyushkin A V 1996 *Phys. Lett.* **B385** 333–342 (*Preprint* hep-ph/9605431)
[4] Ji X D 1997 *Phys. Rev.* **D55** 7114–7125 (*Preprint* hep-ph/9609381)
[5] Collins J C, Frankfurt L and Strikman M 1997 *Phys. Rev.* **D56** 2982–3006 (*Preprint* hep-ph/9611433)
[6] Radyushkin A V 1997 *Phys. Rev.* **D56** 5524–5557 (*Preprint* hep-ph/9704207)
[7] Ji X D and Osborne J 1998 *Phys. Rev.* **D58** 094018 (*Preprint* hep-ph/9801260)
[8] Collins J C and Freund A 1999 *Phys. Rev.* **D59** 074009 (*Preprint* hep-ph/9801262)
[9] Mueller D, Robaschik D, Geyer B, Dittes F M and Horejsi J 1994 *Fortschr. Phys.* **42** 101 (*Preprint* hep-ph/9812448)
[10] Diehl M 2003 *Phys. Rept.* **388** 41–277 habilitation Thesis (*Preprint* hep-ph/0307382)
[11] Polyakov M V 2003 *Phys. Lett.* **B555** 57–62 (*Preprint* hep-ph/0210165)
[12] Belitsky A V and Radyushkin A V 2005 *Phys. Rept.* **418** 1–387 (*Preprint* hep-ph/0504030)
[13] Burkardt M 2000 *Phys. Rev.* **D62** 071503 (*Preprint* hep-ph/0005108)
[14] Ralston J P and Pire B 2002 *Phys. Rev.* **D66** 111501 (*Preprint* hep-ph/0110075)
[15] Miller G A 2007 *Phys. Rev. Lett.* **99** 112001 (*Preprint* 0705.2409)
[16] Burkardt M 2003 *Int. J. Mod. Phys.* **A18** 173–208 (*Preprint* hep-ph/0207047)
[17] Diehl M 2002 *Eur. Phys. J.* **C25** 223–232 (*Preprint* hep-ph/0205208)
[18] Burkardt M 2007 [hep-ph 0711.1881] (*Preprint* 0711.1881)
[19] Guichon P A M and Vanderhaeghen M 1998 *Prog. Part. Nucl. Phys.* **41** 125–190 (*Preprint* hep-ph/9806305)
[20] Belitsky A V, Mueller D and Kirchner A 2002 *Nucl. Phys.* **B629** 323–392 (*Preprint* hep-ph/0112108)
[21] Goeke K, Polyakov M V and Vanderhaeghen M 2001 *Prog. Part. Nucl. Phys.* **47** 401–515 (*Preprint* hep-ph/0106012)
[22] Diehl M, Gousset T, Pire B and Ralston J P 1997 *Phys. Lett.* **B411** 193–202 (*Preprint* hep-ph/9706344)
[23] Belitsky A V and Muller D 2009 *Phys. Rev.* **D79** 014017 (*Preprint* 0809.2890)
[24] Guichon P and Vanderhaeghen M 2008 In preparation
[25] Radyushkin A V 1999 *Phys. Rev.* **D59** 014030 (*Preprint* hep-ph/9805342)
[26] Vanderhaeghen M, Guichon P A M and Guidal M 1999 *Phys. Rev.* **D60** 094017 (*Preprint* hep-ph/9905372)
[27] Polyakov M V and Weiss C 1999 *Phys. Rev.* **D60** 114017 (*Preprint* hep-ph/9902451)
[28] Petrov V Y *et al.* 1998 *Phys. Rev.* **D57** 4325–4333 (*Preprint* hep-ph/9710270)

[29] Guidal M, Polyakov M V, Radyushkin A V and Vanderhaeghen M 2005 *Phys. Rev.* **D72** 054013 (*Preprint* hep-ph/0410251)
[30] Penttinen M, Polyakov M V and Goeke K 2000 *Phys. Rev.* **D62** 014024 (*Preprint* hep-ph/9909489)
[31] Diehl M, Feldmann T, Jakob R and Kroll P 1999 *Eur. Phys. J.* **C8** 409–434 (*Preprint* hep-ph/9811253)
[32] Brodsky S J, Diehl M and Hwang D S 2001 *Nucl. Phys.* **B596** 99–124 (*Preprint* hep-ph/0009254)
[33] Boffi S, Pasquini B and Traini M 2003 *Nucl. Phys.* **B649** 243–262 (*Preprint* hep-ph/0207340)
[34] Ji C R, Mishchenko Y and Radyushkin A 2006 *Phys. Rev.* **D73** 114013 (*Preprint* hep-ph/0603198)
[35] Frankfurt L, Freund A, Guzey V and Strikman M 1998 *Phys. Lett.* **B418** 345–354 (*Preprint* hep-ph/9703449)
[36] Freund A, McDermott M and Strikman M 2003 *Phys. Rev.* **D67** 036001 (*Preprint* hep-ph/0208160)
[37] Polyakov M V and Shuvaev A G 2002 [hep-ph/0207153] (*Preprint* hep-ph/0207153)
[38] Guzey V and Polyakov M V 2006 *Eur. Phys. J.* **C46** 151–156 (*Preprint* hep-ph/0507183)
[39] Guzey V and Teckentrup T 2009 *Phys. Rev.* **D79** 017501 (*Preprint* 0810.3899)
[40] Polyakov M V and Semenov-Tian-Shansky K M 2009 *Eur. Phys. J.* **A40** 181–198 (*Preprint* 0811.2901)
[41] Kumericki K and Mueller D 2010 *Nucl. Phys.* **B841** 1–58 (*Preprint* 0904.0458)
[42] Adloff C *et al.* (H1) 2001 *Phys. Lett. B* **517** 47–58 (*Preprint* hep-ex/0107005)
[43] Aktas A *et al.* (H1) 2005 *Eur. Phys. J.* **C44** 1–11 (*Preprint* hep-ex/0505061)
[44] Aaron F D *et al.* (H1) 2008 *Phys. Lett.* **B659** 796–806 (*Preprint* 0709.4114)
[45] Chekanov S *et al.* (ZEUS) 2003 *Phys. Lett.* **B573** 46–62 (*Preprint* hep-ex/0305028)
[46] Chekanov S *et al.* (ZEUS) 2008 (*Preprint* 0812.2517)
[47] Airapetian A *et al.* (HERMES) 2001 *Phys. Rev. Lett.* **87** 182001 (*Preprint* hep-ex/0106068)
[48] Airapetian A *et al.* (HERMES) 2007 *Phys. Rev.* **D75** 011103 (*Preprint* hep-ex/0605108)
[49] Airapetian A *et al.* (HERMES) 2008 *JHEP* **06** 066 (*Preprint* 0802.2499)
[50] Airapetian A *et al.* (HERMES) 2010 *JHEP* **06** 019 (*Preprint* 1004.0177)
[51] Airapetian A *et al.* (HERMES) 2009 *JHEP* **11** 083 (*Preprint* 0909.3587)
[52] Seitz B (HERMES) 2004 *Nucl. Instrum. Meth.* **A535** 538–541
[53] *Hermes Results On Hard-Exclusive Processes And Prospects Using The New Recoil Detector* in the Proceedings of 11th International Conference on Meson-Nucleon Physics and the Structure of the Nucleon (MENU 2007), Julich, Germany, 10-14 Sep 2007
[54] Stepanyan S *et al.* (CLAS) 2001 *Phys. Rev. Lett.* **87** 182002 (*Preprint* hep-ex/0107043)
[55] Kivel N, Polyakov M V and Vanderhaeghen M 2001 *Phys. Rev.* **D63** 114014 (*Preprint* hep-ph/0012136)
[56] Belitsky A V, Kirchner A, Mueller D and Schafer A 2001 *Phys. Lett.* **B510** 117–124 (*Preprint* hep-ph/0103343)
[57] Mecking B A *et al.* (CLAS) 2003 *Nucl. Instrum. Meth.* **A503** 513–553
[58] Chen S *et al.* (CLAS) 2006 *Phys. Rev. Lett.* **97** 072002 (*Preprint* hep-ex/0605012)
[59] Roblin Y *et al.* (the Hall A DVCS Collaboration) 2000 E00-110 jLab Experiment E00-110, Deeply Virtual Compton Scattering at 6 GeV URL http://hallaweb.jlab.org/experiment/DVCS/dvcs.pdf
[60] Voutier E *et al.* (the Hall A DVCS Collaboration) 2003 E03-106 jLab Experiment E03-106, Deeply Virtual Compton Scattering on the Neutron URL http://hallaweb.jlab.org/experiment/DVCS/dvcs.pdf
[61] Alcorn J *et al.* 2004 *Nucl. Instrum. Meth.* **A522** 294–346
[62] Camsonne A 2005 Ph.D. thesis Université Blaise Pascal, Clermont-Ferrand, France
[63] F Feinstein 2003 *Nucl. Instrum. Meth.* **A504** 258
[64] Munoz Camacho C *et al.* (Jefferson Lab Hall A) 2006 *Phys. Rev. Lett.* **97** 262002 (*Preprint* nucl-ex/0607029)
[65] Mazouz M *et al.* (Jefferson Lab Hall A) 2007 *Phys. Rev. Lett.* **99** 242501 (*Preprint* 0709.0450)
[66] Ahmad S, Honkanen H, Liuti S and Taneja S K 2007 *Phys. Rev.* **D75** 094003 (*Preprint* hep-ph/0611046)
[67] Gockeler M *et al.* (QCDSF) 2004 *Phys. Rev. Lett.* **92** 042002 (*Preprint* hep-ph/0304249)
[68] Brommel D *et al.* (QCDSF-UKQCD) 2007 *PoS* **LAT2007** 158 (*Preprint* 0710.1534)
[69] Hagler P *et al.* (LHPC) 2008 *Phys. Rev.* **D77** 094502 (*Preprint* 0705.4295)
[70] Thomas A W 2008 *Phys. Rev. Lett.* **101** 102003 (*Preprint* 0803.2775)
[71] Camacho C M *et al.* (the Hall A DVCS Collaboration) 2007 JLab E07-007 complete Separation of Deeply Virtual Photon and Neutral Pion Electroproduction Observables of Unpolarized Protons URL www.jlab.org/exp_prog/proposals/07/E07-007.pdf
[72] Mazouz M *et al.* 2008 JLab E08-025 Measurement of the Deeply Virtual Compton Scattering cross-section off the neutron URL www.jlab.org/exp_prog/proposals/08prop.html/PR-08-025.pdf
[73] Girod F X *et al.* (CLAS) 2008 *Phys. Rev. Lett.* **100** 162002 (*Preprint* 0711.4805)
[74] Guidal M 2008 *Eur. Phys. J.* **A37** 319–332 (*Preprint* 0807.2355)
[75] Laget J M 2007 *Phys. Rev.* **C76** 052201 (*Preprint* arXiv:0708.1250[hep-ph])
[76] Burkert V, Elouadrhiri L, Garcon M, Niyazov R, Stepanyan S *et al.* (the CLAS Collabora-

tion) 2006 JLab E06-003 Deeply Virtual Compton Scattering with CLAS at 6 GeV URL http://www.jlab.org/exp_prog/proposals/06/PR06-003.pdf
[77] Biselli A, Elouadrhiri L, Joo K, Niccolai S *et al.* (the CLAS Collaboration) 2005 JLab E05-114 Deeply Virtual Compton Scattering at 6 GeV with polarized target and polarized beam using the CLAS detector URL http://www.jlab.org/exp_prog/proposals/05/PR05-114.pdf
[78] Guidal M 2010 *Phys. Lett.* **B689** 156–162 (*Preprint* 1003.0307)
[79] Klein F, Sandorfi A *et al.* (the CLAS Collaboration) 2006 JLab E06-101 N-star Resonances in Pseudoscalar-meson photo-production from Polarized Neutrons in $\vec{H}\cdot\vec{D}$ and a complete determination of the $\gamma n \to K^0\Lambda$ amplitude URL http://www.jlab.org/exp_prog/proposals/06/PR-06-101.pdf
[80] Berger E R, Cano F, Diehl M and Pire B 2001 *Phys. Rev. Lett.* **87** 142302 (*Preprint* hep-ph/0106192)
[81] Cano F and Pire B 2004 *Eur. Phys. J.* **A19** 423–438 (*Preprint* hep-ph/0307231)
[82] Egiyan H, Girod F X, Hafidi K, Liuti S, Voutier E *et al.* (CLAS) 2008 Deeply Virtual Compton Scattering off ^{4}He JLab E08-024 URL www.jlab.org/exp$_$prog/proposals/08/PR-08-024.pdf
[83] Voutier E Proceedings of the International Workshop on Nuclear Theory, Rila Mountains, Bulgaria, 23-28 Jun 2008 (*Preprint* 0809.2670)
[84] Fenker H C *et al.* 2008 *Nucl. Instrum. Meth.* **A592** 273–286
[85] De Masi R *et al.* (CLAS) 2008 *Phys. Rev.* **C77** 042201 (*Preprint* 0711.4736)
[86] Fuchey E *et al.* (Jefferson Laboratory Hall A) (*Preprint* 1003.2938)
[87] Gilman R, Holt R and Stoler P 2010
[88] Hadjidakis C *et al.* (CLAS) 2005 *Phys. Lett.* **B605** 256–264 (*Preprint* hep-ex/0408005)
[89] Morrow S A *et al.* (CLAS) 2009 *Eur Phys J* **A39** 5–31 (*Preprint* 0807.3834)
[90] Goloskokov S V and Kroll P 2007 *Eur. Phys. J.* **C50** 829–842 (*Preprint* hep-ph/0611290)
[91] Goloskokov S V and Kroll P 2005 *Eur. Phys. J.* **C42** 281–301 (*Preprint* hep-ph/0501242)
[92] Guidal M and Morrow S 2007 Exclusive ρ^0 electroproduction on the proton : GPDs or not GPDs ? [hep-ph 0711.3743] (*Preprint* 0711.3743)
[93] Laget J M 2000 *Phys. Lett.* **B489** 313–318 (*Preprint* hep-ph/0003213)
[94] Cassel D G *et al.* 1981 *Phys. Rev.* **D24** 2787
[95] Airapetian A *et al.* (HERMES) 2000 *Eur. Phys. J.* **C17** 389–398 (*Preprint* hep-ex/0004023)
[96] Adams M R *et al.* (E665) 1997 *Z. Phys.* **C74** 237–261
[97] Chekanov S *et al.* (ZEUS) 2007 *PMC Phys.* **A1** 6 (*Preprint* 0708.1478)
[98] Morand L *et al.* (CLAS) 2005 *Eur. Phys. J.* **A24** 445–458 (*Preprint* hep-ex/0504057)
[99] Joos P *et al.* 1977 *Nucl. Phys.* **B122** 365
[100] Santoro J P *et al.* (CLAS) 2008 *Phys. Rev.* **C78** 025210 (*Preprint* 0803.3537)
[101] Borissov A B (HERMES) 2001 *Nucl. Phys. Proc. Suppl.* **99A** 156–163
[102] Chekanov S *et al.* (ZEUS) 2005 *Nucl. Phys.* **B718** 3–31 (*Preprint* hep-ex/0504010)
[103] Adloff C *et al.* (H1) 2000 *Phys. Lett.* **B483** 360–372 (*Preprint* hep-ex/0005010)
[104] Laget J M 2004 *Phys. Rev.* **D70** 054023 (*Preprint* hep-ph/0406153)
[105] d'Hose N, Burtin E, Guichon P A M and Marroncle J 2004 *Eur. Phys. J.* **A19** Suppl147–53
[106] Moutarde H 2009 *Phys. Rev.* **D79** 094021 (*Preprint* 0904.1648)